Inorg. Chem. **2008**, *47*, 7139−7153

Molybdenum and Tungsten Structural Differences are Dependent on $nd_{z^2}/(n+1)s$ Mixing: Comparisons of $(silox)_3MX/R$ (M = Mo, W; silox = ^{t}Bu$_3$SiO)

David S. Kuiper,[†] Richard E. Douthwaite,[†] Ana-Rita Mayol,[†] Peter T. Wolczanski,*[,†] Emil B. Lobkovsky,[†] Thomas R. Cundari,*[,‡] Oanh P. Lam,[§] and Karsten Meyer[||]

Department of Chemistry & Chemical Biology, Baker Laboratory, Cornell University, Ithaca, New York 14853, Department of Chemistry, Center for Advanced Scientific Computing and Modeling (CASCaM), Box 305070, University of North Texas, Denton, Texas 76203, University of California, San Diego, Department of Chemistry and Biochemistry, 4123 Pacific Hall, 9500 Gilman Drive, La Jolla, California 92093, and University of Erlangen-Nuremberg, Institute of Inorganic Chemistry, Egerlandstr. 1, 91058, Erlangen, Germany

Received January 24, 2008

Treatment of *trans*-$(Et_2O)_2MoCl_4$ with 2 or 3 equiv of Na(silox) (i.e., NaOSi^{t}Bu$_3$) afforded $(silox)_3MoCl_2$ (**1**-Mo) or $(silox)_3MoCl$ (**2**-Mo). Purification of **2**-Mo was accomplished via addition of PMe_3 to precipitate $(silox)_3ClMoPMe_3$ (**2**-MoPMe$_3$), followed by thermolysis to remove phosphine. Use of $MoCl_3(THF)_3$ with various amounts of Na(silox) produced $(silox)_2ClMoMoCl(silox)_2$ (**3**-Mo). Alkylation of **2**-Mo with MeMgBr or EtMgBr afforded $(silox)_3MoR$ (R = Me, **2**-MoMe; Et, **2**-MoEt). **2**-MoEt was also synthesized from C_2H_4 and $(silox)_3MoH$, which was prepared from **2**-Mo and $NaBEt_3H$. Thermolysis of WCl_6 with HOSi^{t}Bu$_3$ afforded $(silox)_2WCl_4$ (**4**-W), and sequential treatment of **4**-W with Na/Hg and Na(silox) provided $(silox)_3WCl_2$ (**1**-W, tbp, X-ray), which was alternatively prepared from *trans*-$(Et_2S)_2WCl_4$ and 3 equiv of Tl(silox). Na/Hg reduction of **1**-W generated $(silox)_3WCl$ (**2**-W). Alkylation of **2**-W with MeMgBr produced $(silox)_3WMe$ (**2**-WMe), which dehydrogenated to $(silox)_3WCH$ (**6**-W) with $\Delta H^{\ddagger} = 14.9(9)$ kcal/mol and $\Delta S^{\ddagger} = -26(2)$ eu. Magnetism and structural studies revealed that **2**-Mo and **2**-MoEt have triplet ground states (GS) and distorted trigonal monopyramid (tmp) and tmp structures, respectively. In contrast, **2**-W and **2**-WMe possess squashed-T_d (distorted square planar) structures, and the former has a singlet GS. Quantum mechanics/molecular mechanics studies of the $S = 0$ and $S = 1$ states for full models of **2**-Mo, **2**-MoEt, **2**-W, and **2**-WMe corroborate the experimental findings and are consistent with the greater $nd_{z^2}/(n+1)s$ mixing in the third-row transition-metal species being the dominant feature in determining the structural disparity between molybdenum and tungsten.

Introduction

The 6s orbital of third-row transition elements is proximate to the 5d orbitals in energy, whereas the 5s orbital is substantially higher than the 4d orbitals for second-row transition elements. These relative energy differences stem from the relativistic contraction of s and p shells in concert with the radial expansion and energetic destabilization (due to increased screening) of d and f shells in the third row.[1] From line spectra, it is estimated that the 6s orbital of tungsten ($[Xe]6s^24f^{14}5d^4$) is >7000 cm^{-1} below the 5d orbitals in energy, whereas the 5s orbital of molybdenum ($[Kr]5s^14d^5$) is about 12 000 cm^{-1} above its 4d orbitals.[2] The ∼19 000 cm^{-1} difference in relative energies can become consequential upon complexation, when $5d_{z^2}$/6s mixing in

* To whom correspondence should be addressed. E-mail: ptw2@cornell.edu (P.T.W.), Fax: 607-255-4137, tomc@unt.edu (T.R.C.), Fax: 940-565-4318.
[†] Cornell University.
[‡] University of North Texas.
[§] University of California, San Diego.
[||] University of Erlangen-Nuremberg.

(1) Pyykkö, P. *Chem. Rev.* **1988**, *88*, 563–594.
(2) (a) Moore. C. E., Ed. *Atomic Energy Levels,, Vol III (National Bureau of Standards, NSRDS-NBS 35)*, U. S. Government Printing Office: Washington D.C., 1971. (b) Oxtoby, D. W.; Gillis, H. P.; Nachtrieb, N. H. , *Principles of Modern Chemistry, 5th Ed.*; Thomson Brooks/Cole: United States, 2002. For a convenient plot of orbital energies vs *Z*, see Figure 15.39 therein.

10.1021/ic800139c CCC: $40.75
Published on Web 07/15/2008

Scheme 1

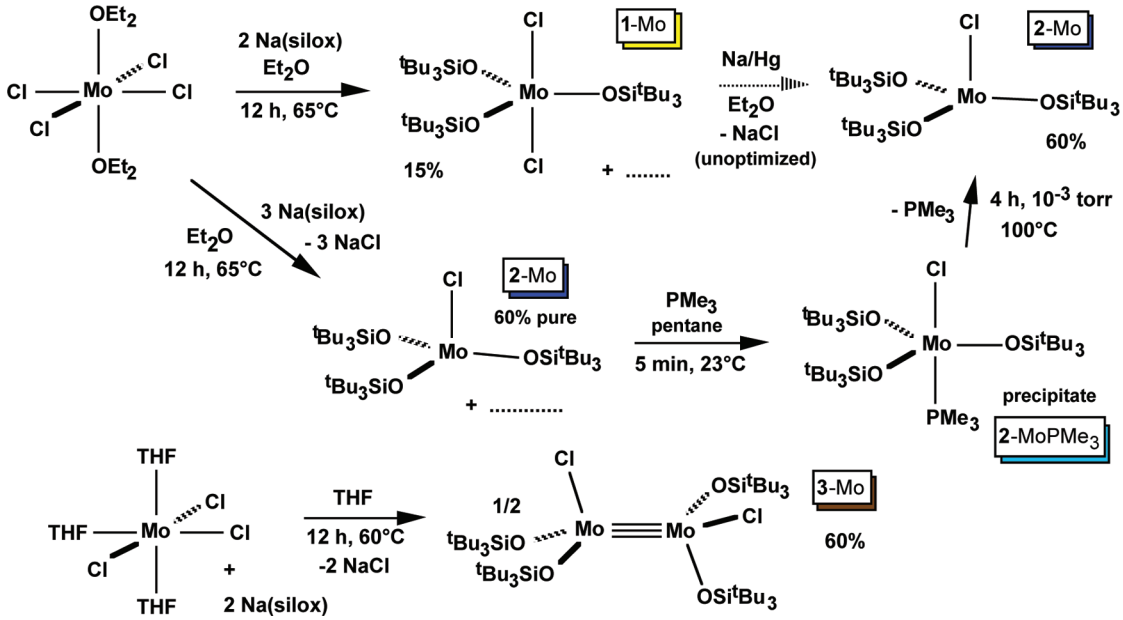

third row complexes lowers the energy of $5d_{z^2}$ to a greater extent than $4d_{z^2}$ is similarly lowered in second-row transition-metal complexes.

Similar metric parameters of 4d and 5d metals (i.e., covalent radii, bond distances, and angles, etc.) can often belie reactivity patterns[3–11] that derive from differences in electronic structure in which $nd_{z^2}/(n+1)$s mixing is critical. For example, different rates of olefin dissociation in $(silox)_3M(olefin)$ and association to $(silox)_3M$ (M = Nb, Ta; silox = ^{t}Bu$_3$SiO) were traced to the higher density of states of niobium versus tantalum.[10] The stability of $(silox)_3Ta$ relative to $(silox)_3Nb$ − a plausible species that has never been directly observed − may stem from the relatively lower energy of $5d_{z^2}$, whose torus is attenuated from mixing with the 6s. Investigations of oxygen atom transfer to d^2 $(silox)_3M$ (M = V, NbL (L = 4-picoline, PMe_3), Ta revealed orbital symmetry constraints in which the energy of the d_{z^2} orbital plays a prominent role.[11]

Previous studies manifested reactivity trends that revealed the importance of $nd_{z^2}/(n+1)$s mixing, but evidence that such electronic factors have an impact on ground-state geometry was lacking. In three-coordinate molecules, changes in the torus of d_{z^2} do not effect the general trigonal geometry observed.[10,11] In higher-coordinate species, the orbital is σ^* and empty, and its filled, bonding counterpart is unlikely to be the origin of a geometric difference. For example, in coordination chemistry studies of biological relevance, molybdenum and tungsten are often complementary in model complexes in part because the metric parameters in relevant 5- and 6-coordinate compounds are so similar.[12–14] In 4-coordinate species, second- and third-row complexes have the capability of exhibiting substantial changes in geometry due to the greater involvement of d_{z^2} in bonding; it may be filled in square planar systems and empty in pseudotetrahedral arrangements, depending on the d^n count. Cummins observed a modest structural effect − a greater planarity for tungsten versus molybdenum in $M(enolate)_4$ species − that hinted at the possibility of greater conformational deviations between second- and third-row transition-metal complexes.[15] Herein is described the synthesis and characterization of a several $(silox)_3MoX/R$ and $(silox)_3WX/R$ compounds that exhibit profound structural differences that can be traced to $nd_{z^2}/(n+1)$s mixing.

Results

Syntheses of $(silox)_3MCl_n$. 1. Molybdenum. As Scheme 1 illustrates, various molybdenum chlorides have been prepared depending on stoichiometry and starting material. Treatment of *trans*-$(Et_2O)_2MoCl_4$[16] with 2 equiv of Na(silox)

(3) (a) Poli, R.; Cacelli, I. *Eur. J. Inorg. Chem.* **2005**, *12*, 2324–2331. (b) Petit, A.; Cacelli, I.; Poli, R. *Chem.—Eur. J.* **2006**, *12*, 813–823.
(4) (a) Carreon-Macedo, J.; Harvey, J. N.; Poli, R. *Eur. J. Inorg. Chem.* **2005**, *12*, 2999–3008. (b) Smith, K. M.; Poli, R.; Harvey, J. N. *Chem.—Eur. J.* **2001**, *7*, 1679–1690.
(5) Carreon-Macedo, J. L.; Harvey, J. N. *J. Am. Chem. Soc.* **2004**, *126*, 5789–5797.
(6) (a) Poli, R. *J. Organomet. Chem.* **2004**, *689*, 4291–4304. (b) Poli, R. *Acc. Chem. Res.* **1997**, *30*, 1861–1866.
(7) (a) Harvey, J. N.; Poli, R.; Smith, K. M. *Coord. Chem. Rev.* **2003**, *238*, 347–361. (b) Poli, R.; Harvey, J. N. *Chem. Soc. Rev.* **2003**, *32*, 1–8. (c) Harvey, J. N.; Poli, R. *Dalton Trans.* **2003**, 4100–4106.
(8) (a) Harvey, J. N. *Struct. Bonding* **2004**, *112*, 151–183. (b) Harvey, J. N. *Phys. Chem. Chem. Phys.* **2007**, *9*, 331–343. (corr. 541)
(9) Matsunaga, N.; Koseki, S. *Rev. Comput. Chem.* **2004**, *20*, 101–152.
(10) K. F., Hirsekorn.; E. B, Hulley.; P. T., Wolczanski.; T. R., Cundari. *J. Am. Chem. Soc.* **2008**, *130*, 1183–1196.
(11) Veige, A. S.; Slaughter, L. M.; Lobkovsky, E. B.; Wolczanski, P. T.; Matsunaga, N.; Decker, S. A.; Cundari, T. R. *Inorg. Chem.* **2003**, *42*, 6204–6224.
(12) Enemark, J. H.; Cooney, J. J. A. *Chem. Rev.* **2004**, *104*, 1175–1200.
(13) (a) Tenderholt, A. L.; Szilagyi, R. K.; Holm, R. H.; Hodgson, K.; Hedman, B.; Solomon, E. *J. Inorg. Biochem.* **2007**, *101*, 1594–1600.
(14) (a) Groysman, S.; Holm, R. H. *Inorg. Chem.* **2007**, *46*, 4090–4102. (b) Wang, J. J.; Tessier, C.; Holm, R. H. *Inorg. Chem.* **2006**, *45*, 2979–2988. (c) Wang, J. J.; Kryatova, O. P.; Rybak-Akimova, E. V.; Holm, R. H. *Inorg. Chem.* **2004**, *43*, 8092–8101. (d) Partyka, D. V.; Staples, R. J.; Holm, R. H. *Inorg. Chem.* **2003**, *42*, 7877–7886.
(15) Soo, H. S.; Figueroa, J. S.; Cummins, C. C. *J. Am. Chem. Soc.* **2004**, *126*, 11370–11376.
(16) Stoffelbach, F.; Saurenz, D.; Poli, R. *Eur. J. Inorg. Chem.* **2001**, 2699–2703.

Scheme 2

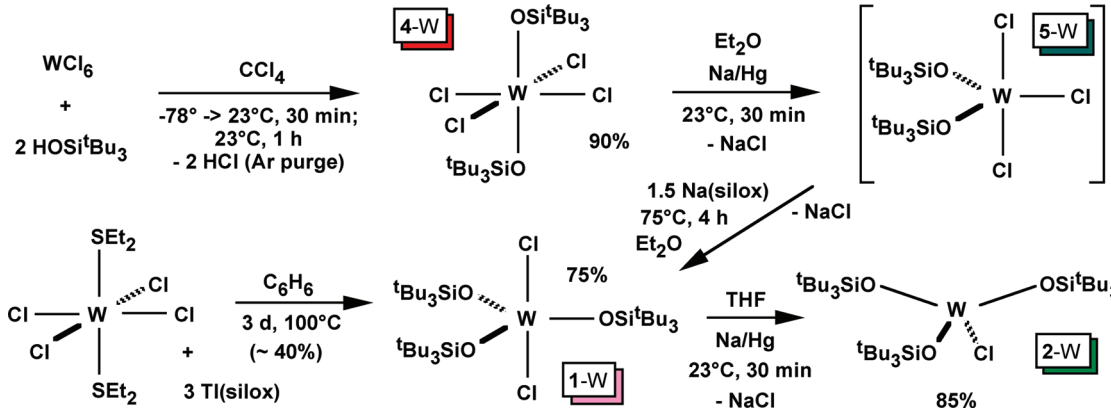

in ether afforded yellow $(silox)_3MoCl_2$ (**1**-Mo) in modest yield (20%) upon crystallization from pentane. The diaxial dichloride trigonal bipyramidal (tbp) structure indicated is based on steric factors and its presumed similarity to the crystallographically characterized tungsten analogue, $(silox)_3WCl_2$ (**1**-W, vide infra). The Mo(V) species exhibited a fairly sharp NMR spectrum (C_6D_6) consisting of a singlet at δ 2.46 ($\upsilon_{1/2}$ = 9 Hz) and a similarly resolved $^{13}C\{^1H\}$ NMR spectrum comprised of CH_3 and SiC resonances at δ 37.27 and 93.68, respectively. Reduction of **1**-Mo produced the desired 4-coordinate derivative, $(silox)_3MoCl$ (**2**-Cl), but isolation proved difficult and a superior method surfaced. Three equiv of Na(silox) and *trans*-$(Et_2O)_2MoCl_4$ produced **2**-Cl in only ~60% purity. However, addition of PMe_3 to a pentane solution cleanly precipitated the aqua PMe_3 adduct, $(silox)_3ClMoPMe_3$ (**2**-MoPMe$_3$). Thermolysis of **2**-MoPMe$_3$ in the solid state at 100 °C for 4 h at 10^{-3} torr released the phosphine, providing blue **2**-Mo in >97% purity and 60% yield based on the tetrachloride. The ^1H NMR spectrum of the Mo(IV) compound revealed a broad signal at δ 3.27 ($\upsilon_{1/2}$ = 30 Hz), and an Evans' method[17] analysis indicated a μ_{eff} of 2.4 μ_B at 23 °C.

While it is tempting to postulate that a disproportionation to Mo(III) and Mo(V) followed by - or during - silox for chloride metathesis would explain the generation of $(silox)_3MoCl_2$ (**1**-Mo) from the Mo(IV) precursor, the reaction of $MoCl_3(THF)_3$[18] with various stoichiometries of Na(silox) generated the brown triply bonded C_2 dimer, $(silox)_2ClMo{\equiv}MoCl(silox)_2$ (**3**-Mo).[19] Since **3**-Mo is not observed in the preparation of **1**-Mo, it is likely that $[(silox)_3MoCl_2]Na$ or $[(silox)_2MoCl_3]Na$ is oxidized in the reaction medium, ultimately resulting in the Mo(V) complex as the major product. Attempts to convert **3**-Mo to $(silox)_3Mo$ or its dimer via metatheses with M(silox) (M = Na, Tl) failed.

2. Tungsten. As shown in Scheme 2, initial approaches to substitution of silox for chloride on tungsten involved treatment of *trans*-$Cl_4W(SEt_2)_2$[20] with M(silox) (M = Na, Tl). With 3 equiv of the favored thallium reagent, the disproportionation to pink, tbp $(silox)_3WCl_2$ (**1**-W) occurred in modest yields (~40%). Fortunately, a better method via W(VI) was developed following Weidenbruch's original silanolysis approach.[21] Tungsten hexachloride was stirred with 2 equiv of $HOSi^tBu_3$ in carbon tetrachloride − accompanied by an argon purge to remove HCl − to afford deep-red $(silox)_2WCl_4$ (**4**-W) in 90% yield. Subsequent reduction of **1**-W with 1 equiv of Na/Hg presumably generated blue-green $(silox)_2WCl_3$ (**5**-W), which was immediately treated with excess Na(silox) to generate **1**-W (75%). Diamagnetic **4**-W exhibited a sharp singlet in its ^1H NMR spectrum at δ 1.38, and paramagnetic **5**-W and **1**-W were characterized by broad singlets at δ 1.61 ($\upsilon_{1/2}$ = 40 Hz) and δ 2.29 ($\upsilon_{1/2}$ = 20 Hz). The overall process provided **1**-W in >60% overall yield, and avoided the use of thallium reagents and the loss of tungsten via redox changes. Reduction of **1**-W with Na/Hg in THF provided the desired 4-coordinate, emerald-green $(silox)_3WCl$ (**2**-W) in 85% yield. Diamagnetic **2**-W manifested a single resonance at δ 1.34 in its ^1H NMR spectrum, and a cooled sample did not further resolve the signal, despite structural evidence (vide infra) that suggested two distinct silox groups.

Structures of $(silox)_3MCl_n$. 1. $(silox)_3MoCl$ (2-Mo). Data collection and crystallographic information for $(silox)_3MoCl$ (**2**-Mo) is listed in Table 1, whereas pertinent bond distances and angles are given in Table 2. As Figure 1 reveals, **2**-Mo adopts a distorted C_{3v} structure between trigonal monopyramidal (tmp)[22,23] and pseudo-tetrahedral geometries, with d(Mo−O) = 1.869(4) $Å_{ave}$, d(Mo−Cl) = 2.2980(10) Å, and O−Mo−O angles of 115.6(5)°$_{ave}$. The only unusual feature to the structure is a decided lean of the molybdenum−chloride bond toward Mo−O2. The Cl−Mo−O2 angle is 98.59(8)° in comparison to the related O−Mo−Cl angles of 104.22(8)°

(17) (a) Evans, D. F. *J. Chem. Soc.* **1959**, 2003–2005. (b) Schubert, E. M. *J. Chem. Educ.* **1992**, *69*, 62.
(18) Dilworth, J. R.; Zubieta, J. *Inorg. Synth.* **1986**, *24*, 193–194.
(19) For tungsten analogues, see:(a) Miller, R. L.; Lawler, K. A.; Bennett, J. L.; Wolczanski, P. T. *Inorg. Chem.* **1996**, *35*, 3242–3253. (b) Miller, R. L.; Wolczanski, P. T.; Rheingold, A. L. *J. Am. Chem. Soc.* **1993**, *115*, 10422–10423. (c) Chamberlin, R. L. M.; Rosenfeld, D. C.; Wolczanski, P. T.; Lobkovsky, E. B. *Organometallics* **2002**, *21*, 2724–2735. (d) Holmes, S. M.; Schafer, D. F., II.; Wolczanski, P. T.; Lobkovsky, E. B. *J. Am. Chem. Soc.* **2001**, *123*, 10571–10583.
(20) King, M. A. S.; McCarley, R. E. *Inorg. Chem.* **1973**, *12*, 1972–1979.
(21) Weidenbruch, M.; Pierrard, C.; Pesel, H. *Z. Naturforsch.* **1978**, *33B*, 1468–1471.
(22) Cummins, C. C.; Lee, J.; Schrock, R. R. *Angew. Chem., Int. Ed. Engl.* **1992**, *31*, 1501–1503.
(23) Veige, A. S.; Wolczanski, P. T.; Lobkovsky, E. B. *Chem. Comm.* **2001**, 2734–2735.

Table 1. Crystallographic Data for (silox)$_3$MoCl (**2**-Mo), (silox)$_3$MoEt (**2**-MoEt), (silox)$_3$WCl$_2$ (**1**-W), (silox)$_3$WCl (**2**-W), and (silox)$_3$WMe (**2**-WMe)

	2-Mo	**2**-MoEt	**1**-W[a]	**2**-W	**2**-WMe
formula	$C_{36}H_{81}O_3Si_3ClMo$	$C_{41}H_{89}O_3Si_3Mo$	$C_{76}H_{170}O_7Si_6Cl_4W$	$C_{36}H_{81}O_3Si_3ClW$	$C_{37}H_{84}O_3Si_3W$
formula wt	777.69	810.36	1874.21	865.60	845.19
space group	$P2_1/n$	$P\bar{1}$	$P2_12_12_1$	$P2_1$	$P2_1/c$
Z	4	2	4	2	4
a, Å	8.6679(4)	8.8484(8)	8.772(3)	8.4736(1)	13.4036(14)
b, Å	21.1749(7)	12.4732(12)	25.076(6)	23.0999(3)	29.592(3)
c, Å	24.2812(8)	22.267(2)	43.581(11)	11.5577(1)	12.6935(13)
α, deg	90	85.315(4)	90	90	90
β, deg	93.856(1)	89.510(4)	90	100.993(1)	118.092(3)
γ, deg	90	77.487(4)	90	90	90
V, Å^3	4446.5(3)	2391.1(4)	9586(5)	2220.78(4)	4441.6(8)
r_{calcd}, g·cm^{-3}	1.162	1.121	1.249	1.294	1.264
μ, mm^{-1}	0.465	0.381	2.624	2.771	2.711
temp, K	173(2)	173(2)	293(2)	173(2)	173(2)
λ (Å)	0.71073	0.71073	0.71073	0.71073	0.71073
R indices [$I > 2\sigma(I)$][b,c]	R1 = 0.0510	R1 = 0.0626	R1 = 0.0655	R1 = 0.0345	R1 = 0.0537
	wR2 = 0.1156	wR2 = 0.1609	wR2 = 0.1397	wR2 = 0.0786	wR2 = 0.1184
R indices (all data)[b,c]	R1 = 0.0811	R1 = 0.0703	R1 = 0.1102	R1 = 0.0451	R1 = 0.0766
	wR2 = 0.1227	wR2 = 0.1667	wR2 = 0.1576	wR2 = 0.0903	wR2 = 0.1271
GOF[d]	1.038	1.017	1.048	1.127	1.063

[a] The formula contains two (silox)$_3$WCl$_2$ molecules and a THF solvent of crystallization. [b] $R1 = \Sigma||F_o| - |F_c||/\Sigma|F_o|$. [c] $wR2 = [\Sigma w(|F_o| - |F_c|)^2/\Sigma wF_o^2]^{1/2}$. [d] GOF (all data) $= [\Sigma w(|F_o| - |F_c|)^2/(n - p)]^{1/2}$, n = number of independent reflections, p = number of parameters.

Table 2. Selected Bond Distances (Angstroms) and Angles (Degrees) for (silox)$_3$MoCl (**2**-Mo) and (silox)$_3$MoEt (**2**-MoEt); Calculated (DFT/MM) Values for Core Features Are Given for Optimized Singlet and Triplet Ground States

	2-Mo	**2**-Mo ($S = 0$)[a]	**2**-Mo ($S = 1$)[a]	**2**-MoEt	**2**-MoEt ($S = 0$)[b]	**2**-MoEt ($S = 1$)[b]
Mo−O1	1.873(2)	1.92	1.92	1.875(2)	1.95	1.95
Mo−O2	1.865(2)	1.91		1.874(2)	1.92	1.94
Mo−O3	1.869(2)	1.91		1.891(2)	1.91	1.93
Mo−Cl	2.2980(10)	2.36	2.36			
Mo−C				2.093(3)	2.18	2.16
CH_2-CH_3				1.491(6)		
O1−Si1	1.670(2)			1.645(2)		
O2−Si2	1.660(2)			1.65092)		
O3−Si3	1.673(2)			1.649(2)		
$(Si-C)_{av}$	1.919(8)			1.92(9)		
$(C-C)_{av}$	1.541(7)			1.54(7)		
O1−Mo−O2	115.18(10)	145	114	117.79(10)	143	120
O1−Mo−O3	115.50(10)	101		118.86(10)	103	119
O2−Mo−O3	116.11(10)	99		118.50(9)	103	115
O1−Mo−Cl	104.22(8)	129	105			
O2−Mo−Cl	98.59(8)	95				
O3−Mo−Cl	104.02(8)	94				
O1−Mo−C				98.23(13)	115	103
O2−Mo−C				97.63(13)	97	100
O3−Mo−C				96.24(12)	94	92
Mo−O1−Si1	165.26(15)			168.22(17)		
Mo−O2−Si2	170.10(16)			166.51(16)		
Mo−O3−Si3	163.53(15)			175.23(15)		
$(O-Si-C)_{av}$	106.0(12)			106.8(20)		
$(C-Si-C)_{av}$	112.7(7)			111(11)		
$(Si-C-C)_{av}$	111.6(13)			111.5(35)		
$(C-C-C)_{av}$	107.2(14)			107.2(47)		

[a] $\Delta H_{ST} = H(S = 0) - H(S = 1) = 11.1$ kcal/mol. [b] $\Delta H_{ST} = H(S = 0) - H(S = 1) = 14.4$ kcal/mol.

and 104.22°; no significant packing interactions can be discerned in unit-cell images. The $^3A_2$ ground-state of a rigorous C_{3v} molecule should not be subject to Jahn−Teller distortions,[24] hence this deviation from 3-fold symmetry is likely to arise from other electronic factors.

2. (silox)$_3$WCl$_2$ (1-W). As expected from steric arguments, (silox)$_3$WCl$_2$ (**1**-W) is a D_{3h} molecule with axial chlorides and equatorial silox groups, as the illustration in Figure 2 depicts. Low-data resolution, and a modest number of reflections, prompted isotropic refinement of peripheral atoms; crystallographic information for **1**-W is given in Table 1. Two independent molecules of **1**-W are found in the asymmetric unit, and their metric parameters are nearly identical. Normal tungsten−oxygen and −chloride distances of 1.823(20) Å (ave) and 2.359(14) Å (av), respectively, are observed, and the O−W−Cl angles average 90.0(9)°. Each

(24) Figgis, B. N.; Hitchman, M. A. *Ligand Field Theory and Its Applications*; Wiley-VCH: New York, 2000.

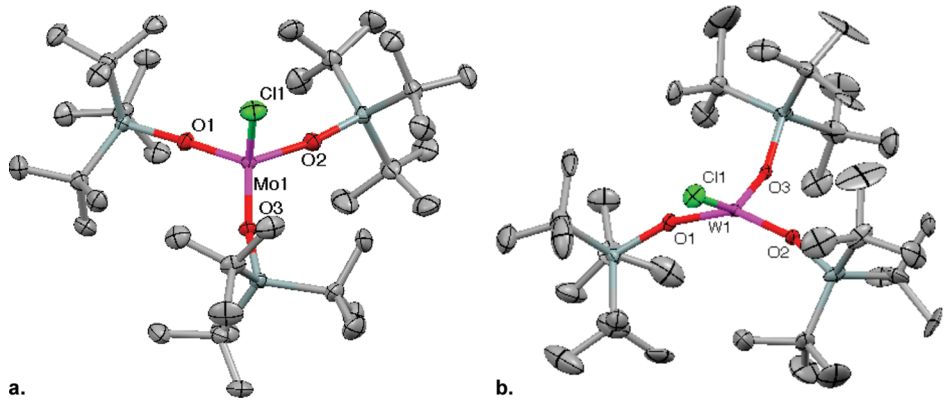

Figure 1. Molecular views of tmp (pseudo T_d) (silox)$_3$MoCl (**2**-Mo) and distorted square planar (or squashed T_d) (silox)$_3$WCl (**2**-W).

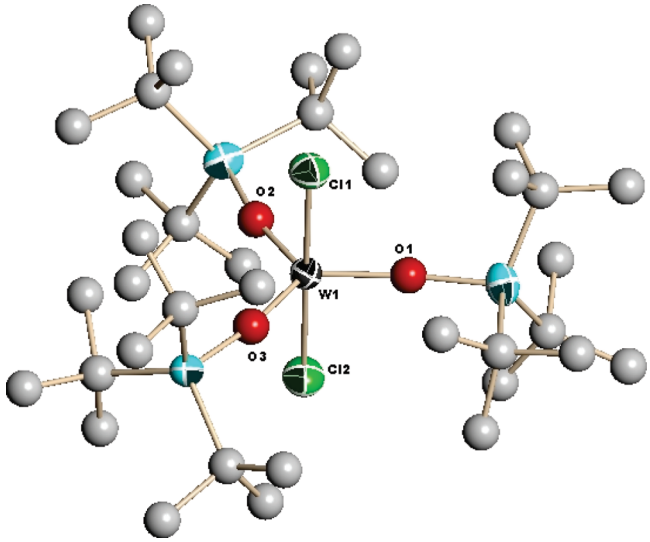

Figure 2. Molecular view of D_{3h} (silox)$_3$WCl$_2$ (**1**-W). Selected bond distances (Å) and angles (°): W1−O1, 1.828(12); W1−O2, 1.786(12); W1−O3, 1.840; W2−O4, 1.826(12); W2−O5, 1.811(12); W2−O6, 1.835(12); W−Cl1, 2.347(7); W−Cl2, 2.382(7); W2−Cl3, 2.353(6); W2−Cl4, 2.355(6); Si−O (av), 1.719(15); O1−W1−O2, 122.8(6); O1−W1−O3, 119.7(6); O2−W1−O3, 117.5(5); O4−W2−O5, 122.3(5); O4−W2−O6, 119.2(5); O5−W2−O6, 118.4(5); O1−W1−Cl1, 88.1(4); O1−W−Cl2, 91.6(4); O2−W1−Cl1, 90.5(5); O2−W1−Cl2, 89.3(5); O3−W1−Cl1, 90.0(4); O3−W1−Cl2, 90.6(4); O4−W2−Cl3, 89.1(5); O4−W2−Cl4, 90.3(5); O5−W2−Cl3, 90.2(4); O5−W2−Cl4, 90.1(4); O6−W2−Cl3, 90.0(5); O6−W2−Cl4, 90.4(5); Cl1−W1−Cl2, 179.4(2); Cl3−W2−Cl4, 179.4(2).

independent molecule possesses an O−W−O angle (122.8(6)° and 122.3(5)°) that is roughly 3σ greater than the remaining ones (119.7(6)°, 117.5(5)°, 119.2(5)°, 118.4°), which could be ascribed to the modest Jahn−Teller distortion[24] expected for the ^{2}E″ ground-state of **1**-W.

3. (silox)$_3$WCl (2-W). Crystallographic information for (silox)$_3$WCl (**2**-W) is given in Table 1, whereas bond distances and angles are listed in Table 3. As Figure 1 reveals, the structure of **2**-W is decidedly different than its molybdenum analogue, consistent with its diamagnetic behavior. The d(W−O), which averages 1.865(8) Å, and the tungsten−chloride bond of 2.3380(10) Å, represent normal distances, but the core angles deviate substantially from either tetrahedral or square planar geometries. Two Cl−W−O angles average 89.2(12)°, whereas the third is 139.73(8). Likewise, two O−W−O angles average 101(2)° but the third is 148.19(14)°; thus, the geometry can be considered as squashed T_d or distorted square planar. Two opposing W−O−Si linkages are bent to one side of the pseudosquare plane, whereas the silox opposite the chloride is bent down and away from the others in response to steric factors.

Derivatives of (silox)$_3$MCl$_n$. 1. Molybdenum. In 4-coordinate molecules containing a 3-fold axis, the energy of d_{z^2} can be readily changed via substitution, thus alkyl derivatives of (silox)$_3$MoCl (**2**-Mo) were sought to see whether a structural change could be effected. Treatment of **2**-Mo with either MeMgBr or EtMgBr in Et$_2$O provided the red-brown Me and green Et derivatives, (silox)$_3$MoR (R = Me, **2**-MoMe; Et, **2**-MoEt) in ∼70% yield, as shown in Scheme 3. The ^{1}H NMR spectrum for **2**-MoMe showed one paramagnetic resonance at δ 2.88 ($\upsilon_{1/2}$ = 76 Hz); the methyl group was not observed. Likewise, **2**-MoEt exhibited a resonance at δ 2.77 ($\upsilon_{1/2}$ = 68 Hz), but no other signals were seen in its ^{1}H NMR spectrum. The brown-green hydride, (silox)$_3$MoH (**2**-MoH) was also prepared metathetically via the addition of Na[Et$_3$BH] to **2**-Mo, and subsequently exposed to an excess of ethylene (10 equiv) to afford an alternate route to **2**-MoEt. **2**-MoH also exhibited a υ(MoH) of 1884 cm^{-1} in its IR spectrum characteristic of a terminal hydride. Evans' method measurements[17] on the three paramagnetic derivatives (23 °C) revealed a μ_{eff} of 2.5 μ_B for **2**-MoMe and **2**-MoEt and a μ_{eff} of 2.6 μ_B for **2**-MoH.

2. Tungsten. Derivatization of (silox)$_3$WCl (**2**-W) was accomplished via metathesis with MeMgBr to produce the purple methyl complex, (silox)$_3$WCH$_3$ (**2**-WMe) in ∼40% yield as illustrated in Scheme 4. Whereas **2**-WMe was expected to be possess a singlet ground-state like the precursor chloride, its ^{1}H NMR exhibited a single broad resonance at δ 3.69 ($\upsilon_{1/2}$ = 6 Hz; WMe not observed); in addition, an Evans' method measurement revealed a μ_{eff} of 1.5 μ_B. The magnetic moment is substantially less than expected for a d^2 system and might be indicative of a singlet ground-state in thermal equilibrium with a triplet excited state, or temperature-independent paramagnetism (TIP). Unfortunately, full magnetic studies have been hampered by the instability of **2**-WMe, which loses dihydrogen, even in the solid state. A kinetics study of the quantitative conversion of **2**-WMe to the yellow-green alkylidyne, (silox)$_3$WCH (**6**-W), yielded activation parameters of $\Delta H^{\ddagger}$ = 14.9(9) kcal/mol and $\Delta S^{\ddagger}$ = −26(2) eu (Scheme 4). The transition state

Table 3. Selected Bond Distances (Angstroms) and Angles (Degrees) for $(silox)_3WCl$ (**2**-W) and $(silox)_3WMe$ (**2**-WMe); Calculated (DFT/MM) Values for Core Features Are Given for Optimized Singlet and Triplet Ground States

	2-W	**2**-W ($S = 0$)[a]	**2**-W ($S = 1$)[a]	**2**-WMe	**2**-WMe ($S = 0$)[b]	**2**-WMe ($S = 1$)[b]
W−O1	1.872(4)	1.90	1.93	1.851(4)	1.92	1.93
W−O2	1.865(5)	1.90	1.91	1.853(4)	1.90	1.93
W−O3	1.857(2)	1.89	1.90	1.885(4)	1.90	1.92
W−Cl	2.3380(10)	2.36	2.36			
W−C				2.060(7)	2.14	2.14
O1−Si1	1.712(4)			1.659(5)		
O2−Si2	1.656(5)			1.667(4)		
O3−Si3	1.702(3)			1.675(5)		
$(Si-C)_{av}$	1.93(4)			1.909(10)		
$(C-C)_{av}$	1.56(3)			1.54(2)		
O1−W−O2	148.19(14)	148	118	142.0(2)	149	122
O1−W−O3	99.1(3)	100	116	104.99(16)	102	117
O2−W−O3	102.6(3)	98	108	104.91(17)	101	114
O1−W−Cl	90.0(2)	136	113			
O2−W−Cl	88.3(2)	93	106			
O3−W−Cl	139.73(8)	91	94			
O1−W−C				91.2(2)	130	107
O2−W−C				90.7(2)	92	97
O3−W−C				124.5(3)	90	93
W−O1−Si1	159.0(2)			164.8(3)		
W−O2−Si2	165.2(3)			164.3(4)		
W−O3−Si3	150.3(2)			155.0(3)		
$(O-Si-C)_{av}$	106(2)			106.2(15)		
$(C-Si-C)_{av}$	112(8)			112.5(8)		
$(Si-C-C)_{av}$	111(4)			111.8(18)		
$(C-C-C)_{av}$	108(5)			107.0(14)		

[a] $\Delta H_{ST} = H(S = 0) - H(S = 1) = 0.2$ kcal/mol. [b] $\Delta H_{ST} = H(S = 0) - H(S = 1) = 2.9$ kcal/mol.

Scheme 3

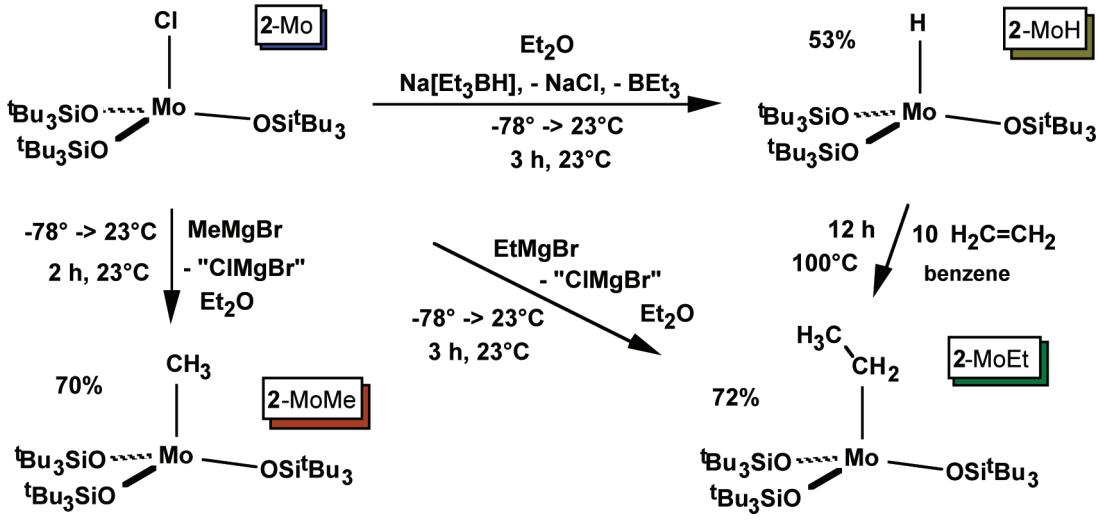

for H_2 loss is highly ordered, as was established for previous dehydrogenations of group 6 alkyls by Schrock et al.[25]

Structures of $(silox)_3MR$. 1. $(silox)_3MoEt$ (2-MoEt). Crystals of diffraction quality were more easily obtained for the molybdenum ethyl derivative, $(silox)_3MoEt$ (**2**-MoEt), than the corresponding methyl species. Data collection and refinement information is provided in Table 1, and the metric parameters are given in Table 2. Part a of Figure 3 shows that **2**-MoEt possesses clear 3-fold symmetry and is closer to a trigonal monopyramid (tmp) than a tetrahedron based on O−Mo−O angles that average 118.4(5)° and O−Mo−C angles that average 97.4(10)°. The Et group does not exhibit the cant that the chlorine exhibits in $(silox)_3MoCl$ (**2**-Mo). Normal d(MoO) of 1.880(10) Å (ave) are found and the Mo−C distance is 2.093(3) Å, which is near the sum of covalent radii (2.07 Å) and typical for Mo(IV).

2. $(silox)_3WMe$ (2-WMe). Crystallographic information for $(silox)_3WMe$ (**2**-WMe) is given in Table 1, and a listing of distances and angles is given in Table 3. As part b of Figure 3 illlustrates, **2**-WMe adopts the squashed-T_d (or distorted square planar) geometry seen for $(silox)_3WCl$ (**2**-W), albeit with subtle differences. The tungsten−oxygen distances average 1.863(19) Å and the tungsten−carbon

(25) (a) Schrock, R. R.; Seidel, S. W.; MoschZanetti, N. C.; Shih, K. Y.; ODonoghue, M. B.; Davis, W. M.; Reiff, W. M. *J. Am. Chem. Soc.* **1997**, *119*, 11876–11893. (b) Schrock, R. R.; Seidel, S. W.; MoschZanetti, N. C.; Dobbs, D. A.; Shih, K. Y.; Davis, W. M. *Organometallics* **1997**, *16*, 5195–5208. (c) Seidel, S. W.; Schrock, R. R.; Davis, W. M. *Organometallics* **1998**, *17*, 1058–1068.

Scheme 4

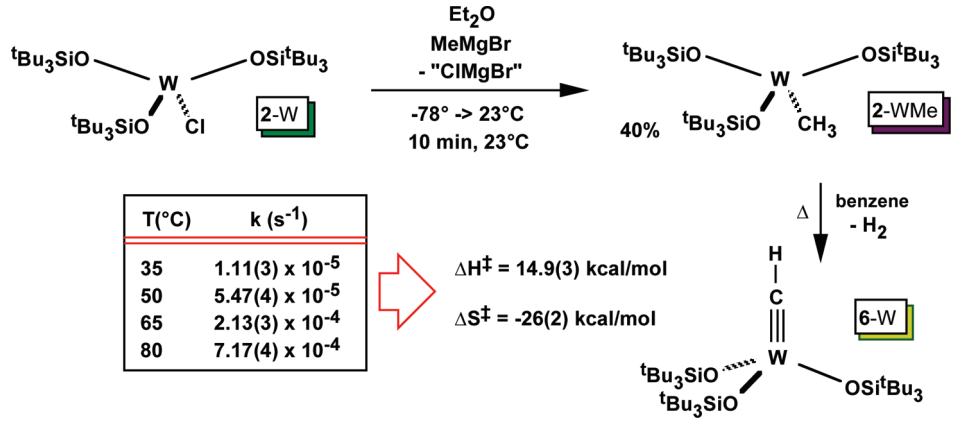

distance is 2.060(7); both are quite typical for W(IV). The core angles of **2**-WMe differ from the chloride by being somewhat closer to tetrahedral. The O1−W−O3 and O2−W−O3 angles are 104.99(16)° and 104.91(17)°, whereas the corresponding angles in **2**-W are 99.1(3)° and 102.6(3)°. The differences are most obvious in the trans C−W−O3 and O1−W−O2 angles of 124.5(3)° and 142.0(2)°, respectively, which are substantially less than those of **2**-W (139.73(8)° and 148.19(14)°). The remaining core angles, O1−W−C and O2−W−C, are 91.2(2)° and 90.7(2)°, respectively.

Magnetic Studies of (silox)$_3$MoX (X = Cl, 2-Mo; Et, 2-MoEt). Temperature-dependent magnetic susceptibility studies were conducted on (silox)$_3$MoCl (**2**-Mo) and (silox)$_3$MoEt (**2**-MoEt) to determine whether their relatively low moments were indicative of unusual behavior. Plots of M/H versus T for **2**-Cl and μ_{eff} versus T shown in Figure 4 reveal simple paramagnetic behavior from roughly 50−300K. The μ_{eff} is relatively constant at $\mu_{eff} = 2.5(2)\ \mu_B$, a value less than spin-only due to orbital contributions to the moment, as predicted for a d^2 system. At less than 50 K, the susceptibility declines and μ_{eff} decreases toward ~0.6 μ_B as the effect of zero-field splitting − a combination of spin−orbit coupling and low-symmetry effects − reveals itself. The ethyl derivative, **2**-Et, manifests related behavior, although the μ_{eff} from ~50−300 K is slightly higher (2.6(1) μ_B, Figure 5). The susceptibilities of **2**-Mo and **2**-MoEt are consistent with the pseudo-tmp geometry observed for the two complexes.

Discussion

Molybdenum and Tungsten Structures. When the coordination number is restricted to 4 in a d^2 system, the energy of d_{z^2} must play a prominent role in establishing the geometry of the complex. In this study, the lower energy of the $5d_{z^2}$ orbital − due to mixing with the 6s − allows it to be filled in the squashed-T_d conformation, whereas the purer $4d_{z^2}$ orbital of the second-row transition metal is essentially σ^* and empty. Even-greater perturbation by an alkyl in (silox)$_3$MoEt (**2**-MoEt) relative to (silox)$_3$MoCl (**2**-Mo) does not increase the field strength enough to change the conformation from tmp. The magnetic behavior of **2**-Mo and **2**-MoEt from 5 to 300 K is consistent with the low symmetry of both species and reflects the expected zero-field splitting. To support the above arguments, high-level quantum computations were conducted to probe the electronic basis of the structure changes from molybdenum to tungsten.

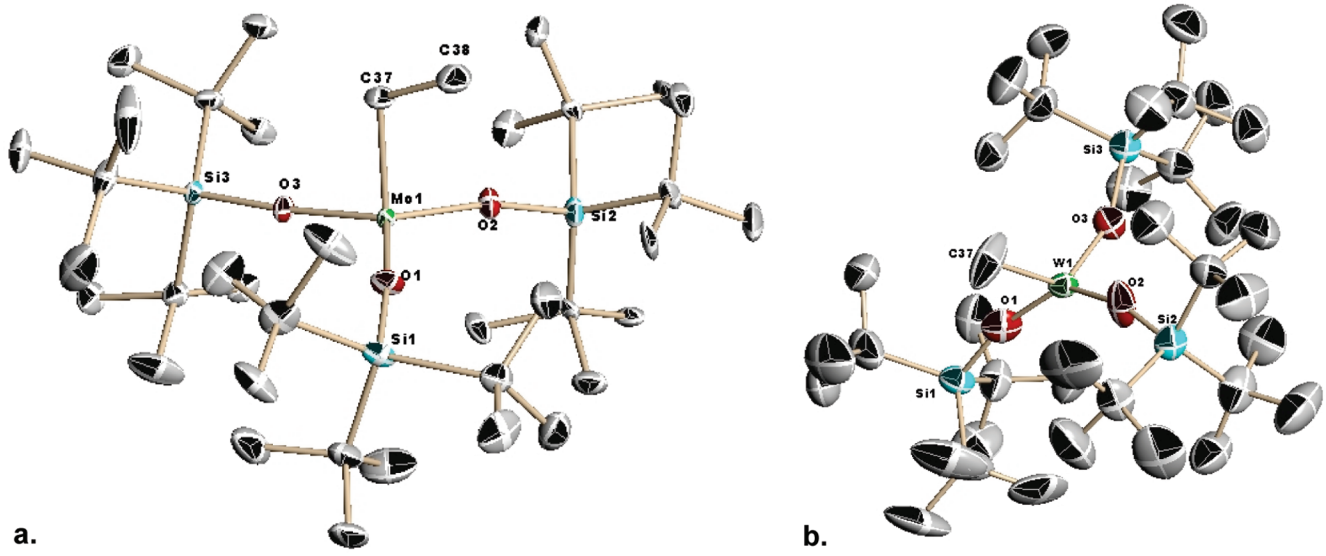

Figure 3. Molecular views of tmp (pseudo T_d) (silox)$_3$MoEt (**2**-MoEt) and distorted square planar (or squashed T_d) (silox)$_3$WMe (**2**-WMe).

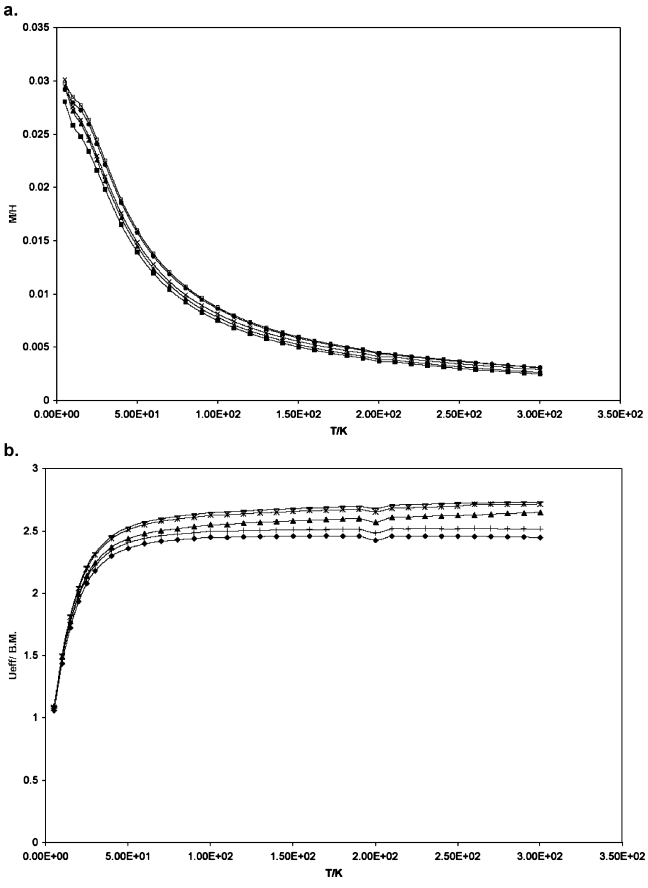

Figure 4. (a) M/H vs T plots for $(silox)_3MoCl$ (**2**-Cl) generated from 5 runs using 3 different samples. (b) μ_{eff} vs T plots for **2**-Cl corresponding to those in a.

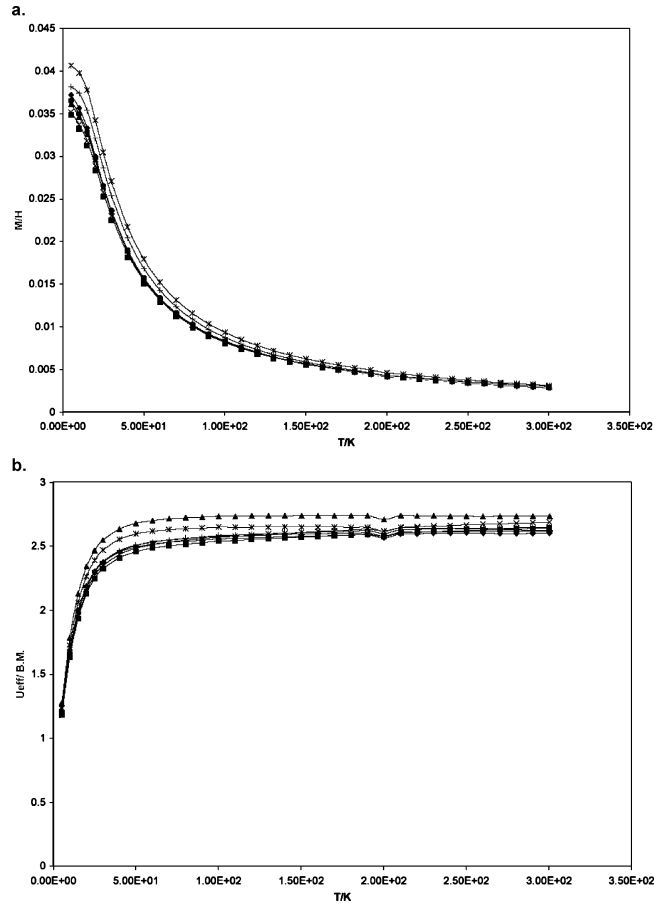

Figure 5. a. M/H vs T plots for $(silox)_3MoEt$ (**2**-MoEt) generated from 7 runs using 3 different samples. b. μ_{eff} vs T plots for **2**-MoEt corresponding to those in a.

Calculations. 1. Singlet and Triplet $(silox)_3MCl$ (M = Mo, 2-Mo; W, 2-W). A hybrid quantum mechanics/molecular mechanics approach enabled calculations of the complexes with the complete silox ligands.[11,26–31] Calculated core metric parameters for $(silox)_3MoCl$ (**2**-Mo; $S = 0$, 1) are listed in Table 2, where it is readily seen that the observed (X-ray) geometry correlates with the triplet configuration, although the calculated bond distances are significantly longer than those found experimentally. The d orbitals and their energies in both the singlet and triplet configurations are given in Figure 6. In this illustration, note that the absolute energies of molybdenum versus tungsten orbitals are not comparable, and even those pertaining to the $S = 0$ and $S = 1$ configurations of the same transition metal must be carefully interpreted, because filled core orbitals are critical to the overall electronic energies of the molecules.

As stated in Table 2, the $S = 1$ state corresponding to the tmp (pseudo-T_d) $(silox)_3MoCl$ (**2**-Cl) geometry is roughly 11 kcal/mol lower (0.48 eV) than the corresponding $S = 0$ state of the squashed-T_d geometry. The unpaired electrons occupy essentially d_{xz} and d_{yz} orbitals in a tmp field that is extremely weak, spanning only 0.52 eV in energy compared to the 2.15 eV spread attributed to the singlet. Whereas the orbital designations for the triplet are conventional, the low symmetry of the squashed-T_d singlet configuration renders these orbitals highly mixed, but at least the lowest orbital clearly has the dominant character of d_{z^2}. If we assume the Mo−O and Mo−Cl bonds in the two configurations are energetically similar − and the core orbital energies are correspondingly similar (essentially an angular overlap model (AOM) estimate)[24] − then the 2 K of exchange energy and lesser Coulomb energy of the triplet state must overcome (by ∼19 000 cm^{-1} or ∼2.4 eV) the greater stabilization of the $(d_{z^2})^2$ configuration of the singlet state, which is ∼15 000 cm^{-1} (∼1.9 eV) lower in orbital energy relative to the $(d_{xz})^1(d_{yz})^1$ configuration of the triplet. Although these numbers probably overestimate the singlet−triplet (S/T) energy difference,[3] there is little doubt that the spatial characteristics of the occupied orbitals of the two states play a critical role in ultimately favoring the triplet. Whereas it is germane to compare the tmp $S = 1$ state to the squashed-T_d $S = 0$ state, it must be noted that there are triplet states of similar energy in the latter geometry for **2**-Mo.

As the footnotes in Table 3 state, the energies of the singlet (squashed-T_d) and triplet (tmp or pseudo-T_d) forms of $(silox)_3WCl$ (**2**-W) are calculated to be essentially the same, although the experimental metric parameters and diamagnetism clearly reveal the $S = 0$ state to be lower in energy. The $S = 1$ state is calculated to be slightly less symmetrical than the corresponding molybdenum configuration, and the dispersion of orbital energies is higher (0.93 eV vs 0.52 eV (molybdenum)) due to this asymmetry and the ∼1.0−1.5 greater field strength typical for a third-

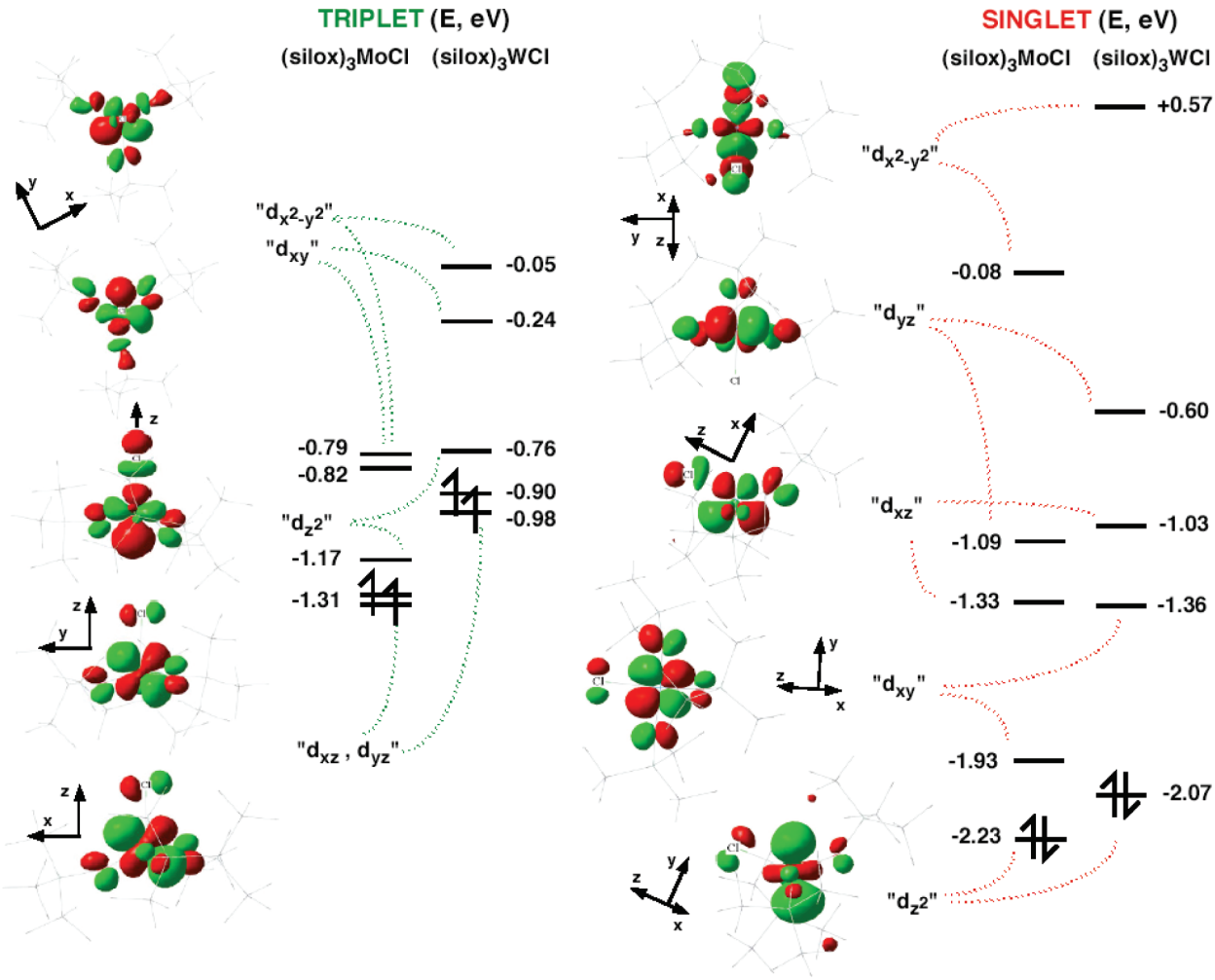

Figure 6. Orbitals (red and green) and their energies (1 eV = 8065.5 cm^{-1}) of triplet and singlet $(silox)_3MCl$ (M = Mo, **2**-Mo; W, **2**-W). Orbitals shown for the triplets are those of **2**-Mo; those of **2**-W are very similar. Orbitals shown for the singlets are those of **2**-W; those of **2**-Mo are very similar.

row transition element relative to its second-row congener.[24] The stronger field $S = 0$ squashed-T_d configuration also displays orbital energies that span 2.64 eV as compared to 2.15 eV for molybdenum. The similarities in geometry between **2**-Mo and **2**-W for the two states suggest that the same arguments can be applied to tungsten; the 2 K of exchange energy of the $(d_{xz})^1(d_{yz})^1$ configuration of the $S = 1$ state and its lesser Coulomb energy should be ~19 000 cm^{-1} (~2.4 eV) The orbital energy of the $(d_{z^2})^2$ state should be ~19 000 cm^{-1} lower than that of the triplet; it is ~18 000 cm^{-1} (~2.2 eV) lower, which is quite satisfactory given the same assumptions as above. In this study, singlet−triplet (S/T) estimates are used to show the consistency of the calculations regarding molybdenum and tungsten; the actual energies are likely to be overestimated.[3]

What is the origin of the change in structure from the tmp of **2**-Mo to the squashed T_d of **2**-W? For the tungsten case, note that d_{z^2} is relatively lower to the other d orbitals when compared to molybdenum. This is perhaps most readily seen by comparing the energy of d_{z^2} in the $S = 1$ state to its energy in the $S = 0$ state. For **2**-Mo, the energy lowering of $4d_{z^2}$ is 1.06 eV, whereas $5d_{z^2}$ is lowered by 1.31 eV for **2**-W, and this is the dominant *relative energy factor* that determines the change in structure. The different relative energies can be considered a consequence of the greater $nd_{z^2}/(n + 1)s$ mixing of the third-row transition element relative to the second-row species. The difference in d_{z^2} orbital energies is revealed to a greater extent in the pseudo square-planar (squashed-T_d) environment, where mixing attenuates the torus and removes more antibonding character relative to the tmp geometry.

2. Singlet and Triplet $(silox)_3MR$ (M = MoEt, 2-MoEt; WMe, 2-WMe). As given in Table 2, the $S = 1$ state of tmp $(silox)_3MoEt$ (**2**-MoEt) is calculated to be ~14 kcal/mol (~5000 cm^{-1}, 0.62 eV) more favorable than the $S = 0$ state of the squashed-T_d structure. Again, the computed structure is consistent with the experimental one, but the metric parameters of the calculated tmp (or pseudo-T_d) species have significantly longer bond lengths, and there are modest distortions from 3-fold symmetry. The triplet state of $(silox)_3WMe$ (**2**-WMe) is calculated to be marginally (~3 kcal/mol, ~0.1 eV) more stable than the squashed-T_d $S = 0$ state. Whereas this appears to corroborate the paramagnetic character of **2**-WMe, the experimental structural parameters (Table 3) are better fit by the calculated $S = 0$ species; the calculated bond lengths are long for both the singlet and the triplet. The low experimental moment for **2**-WMe at 23 °C

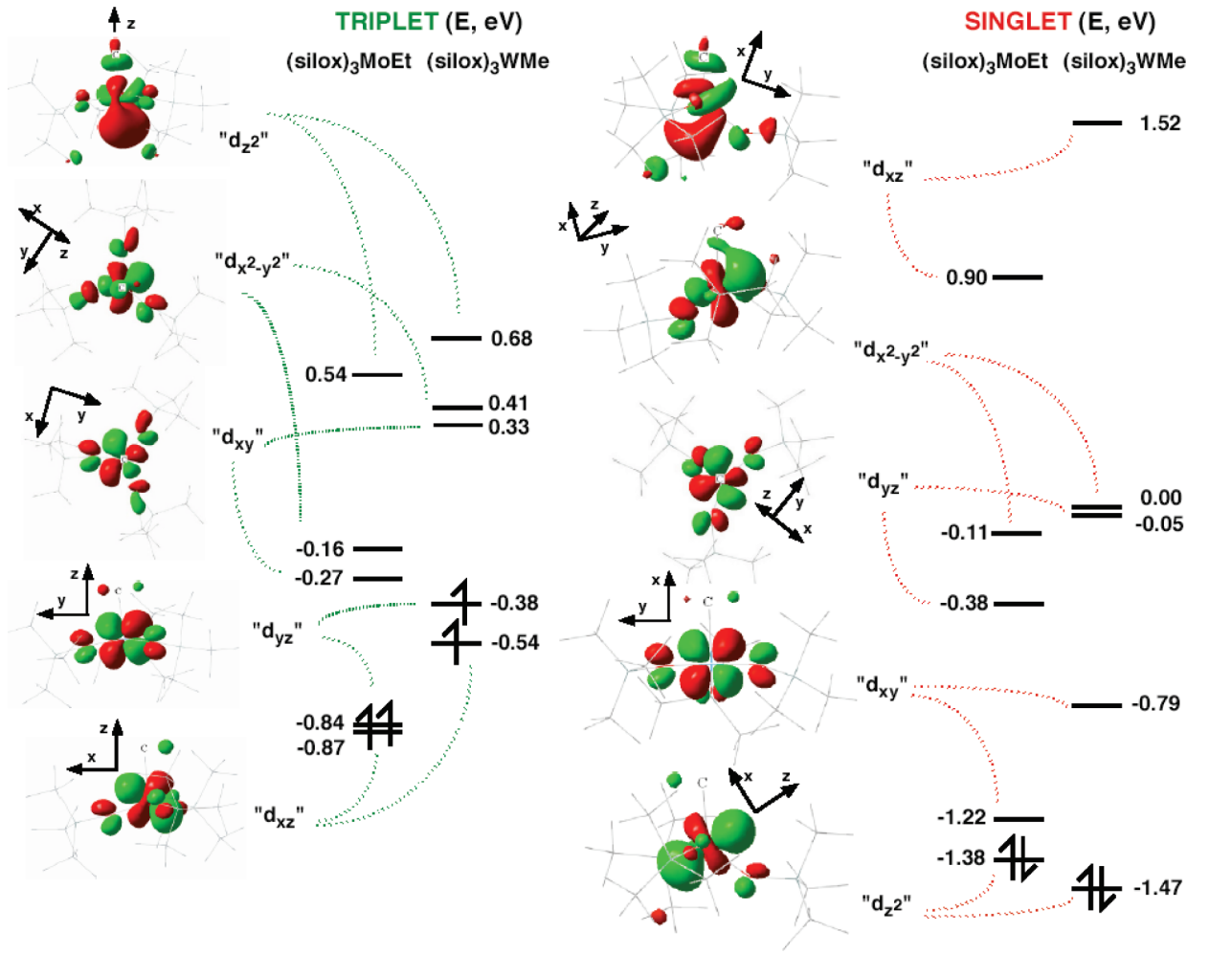

Figure 7. Orbitals (red and green) and their energies (1 eV = 8065.5 cm^{-1}) of triplet and singlet $(silox)_3MR$ (MR = MoEt, **2**-MoEt; WMe, **2**-WMe). Orbitals shown for the triplets are those of **2**-MoEt; those of **2**-WMe are very similar. Orbitals shown for the singlets are those of **2**-WMe; those of **2**-MoEt are very similar.

(μ_{eff} = 1.5 μ_B) may be indicative of close singlet and triplet states within the squashed-T_d geometry; the ground-state could be $S = 0$, and the magnetism purely temperature-independent paramagnetism (TIP).

As expected for the stronger field imparted by the alkyl, the orbital energy dispersion in the alkyls is significantly greater than that in the chlorides, as Figure 7 reveals. The field for **2**-MoEt is spread over 1.41 eV, and this is surprisingly larger than the 1.22 eV spread for **2**-WMe. It is conceivable that the donor capability of Et versus Me may be partly responsible for this difference, but what is certain is that d_{z^2} is far higher in energy in the molybdenum case relative to d_{xy}, the next highest orbital. This order is different than in the $S = 1$ chlorides, where the d_{z^2} orbital was quite low, giving the appearance of a 2 over 3 orbital field rather than the 3 over 2 arrangement normally seen for pseudo-T_d species.[24] The alkyls thus appear more normal in the d-orbital splitting diagram.

The orbital energy of the $(d_{z^2})^2$ configuration for singlet **2**-MoEt is ~8500 cm^{-1} (~1.1 eV) more favorable than the $(d_{xz})^1(d_{yz})^1$ configuration of the $S = 1$ state, whose 2 K of exchange energy and better Coulomb energy of ~13 500 cm^{-1} (~1.7 eV) must overcome this disadvantage, given the aforementioned assumptions. The value is less than in the chloride cases, possibly due to the expanded field of the alkyl derivatives. The $S = 0$ state for **2**-W has an orbital energy that is ~16 000 cm^{-1} (2.0 eV) more favorable than that of the triplet state. There is a modest discrepancy here in that the triplet is calculated to be more stable by 2.9 kcal/mol (~1000 cm^{-1}, ~0.12 eV), hence exchange and Coulomb effects should be around ~17 000 cm^{-1}, but with given the assumptions in these simple arguments, the accuracy is acceptable.

In accord with the higher-field-strength alkyls, the orbital energy dispersion of the $S = 0$ state of the squashed-T_d pertaining to **2**-MoEt spans 2.28 eV, and that of **2**-WMe covers 2.99 eV. The former value is essentially the same as **2**-Mo, hence the supposed stronger field imparted by the alkyl seems to have had little effect on the orbital energy dispersion in the squashed-T_d geometry. Upon changing from tmp ($S = 1$) to the squashed-T_d ($S = 0$) structure, the energy of the $4d_{z^2}$ orbital in **2**-MoEt is lower by 1.92 eV, and the $5d_{z^2}$ orbital in **2**-WMe is similarly lower by 2.15 eV. This is roughly the same difference as in the chlorides and can again be attributed to the greater $nd_{z^2}/(n + 1)s$ mixing of the third-row transition element relative to its second-row congener.

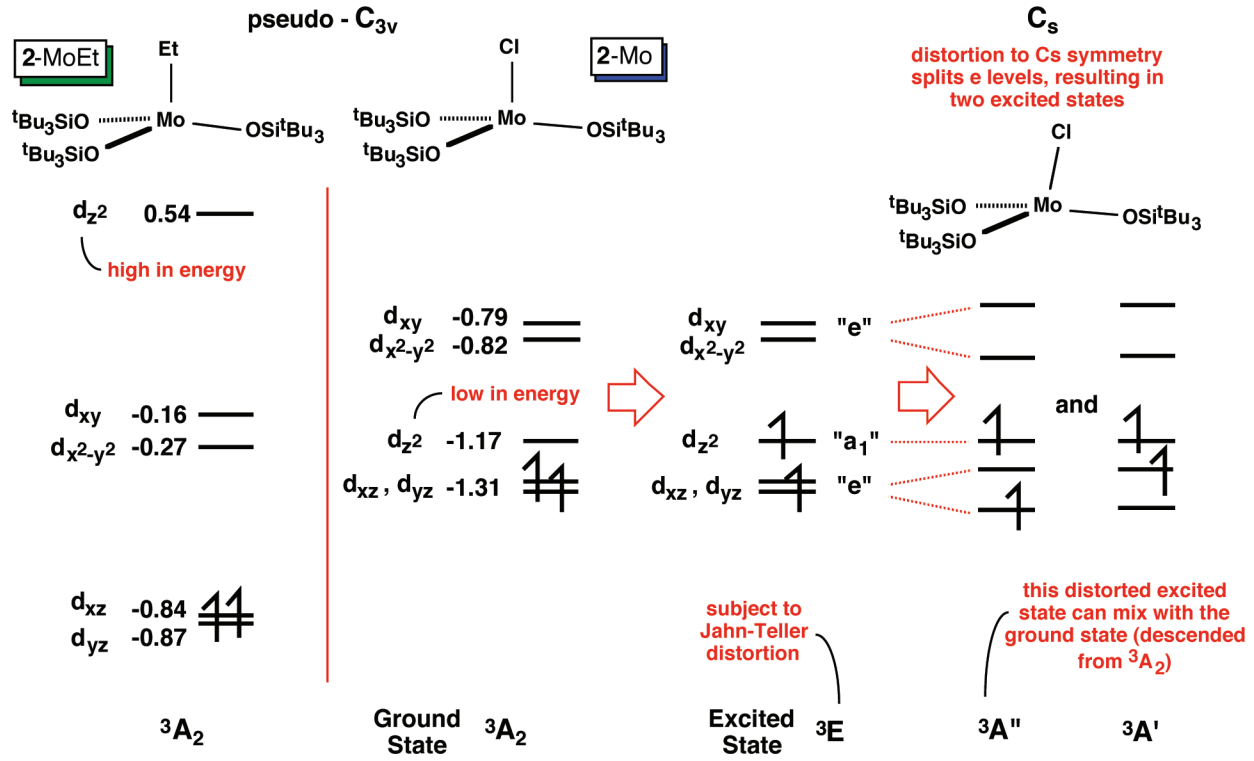

Figure 8. The low-lying $4d_{z^2}$ orbital in $(silox)_3MoCl$ (**2**-Mo) suggests that low-lying excited states derived from an $(e)^1(a_1)^1$ configuration (i.e., $(d_{xz})(d_{yz})^1(d_{z^2})^1$) in C_{3v} should Jahn−Teller distort to C_s symmetry; mixing of the appropriated excited-state with the $^3A_2$ ground state (GS) of **2**-Mo (C_{3v}) provides the means for the observed GS distortion (Renner−Teller).

The Mo−Cl Lean in $(silox)_3MoCl$ (2-Mo). The calculations failed to reproduce the asymmetry of the $(silox)_3MoCl$ (**2**-Mo) complex, whose origin appears to be electronic because no significant intermolecular interactions were discerned from the X-ray study. As Figure 8 illustrates, the d_{z^2} orbital of **2**-Mo is quite low and near the d_{xz}, d_{yz} set that is half-occupied in the triplet configuration, according to the calculations. The occupation of d_{z^2} results in a low-lying excited state (^3E in C_{3v}) that is subject to Jahn−Teller distortion,[24] whereas the $^3A_2$ ground state (C_{3v}) is not. For comparison, the d_{z^2} in $(silox)_3MoEt$ (**2**-MoEt) is energetically high, and any excited-state in which this orbital is occupied would be separated from the ground state by a large amount of energy. The Jahn−Teller distortion of the ^3E excited state leads to two excited states in C_s symmetry; one of these has the appropriate symmetry to mix with the $^3A_2$ ground state. This mixing of an excited state with a ground state that results in a distortion is in essence a Renner−Teller effect,[32] usually attributed to distortions of linear molecules. The proximity of d_{z^2} to the e set in **2**-Mo permits this interaction, whereas **2**-MoEt retains its 3-fold symmetry, as is observed. It is uncertain why the calculations do not pick up this asymmetry, but it is probable that the effect is highly dependent on the basis set, electronic structure methodology chosen, and the proximity of d_{z^2}, hence it may be easily missed.

Perspective. Outside of Cummins' tetraenolate investigation of molybdenum and tungsten,[16] comparison studies of this type are not common, especially when restricted to 4-coordination. There are, however, a select number of d^2 4-coordinate molecules that are germane to this work. For example, Schrock's investigations of $(ArN=)_2WLL'$[33,34] and $(ArN=)_2ReXL$[34,35] compounds show that these derivatives do not stray from pseudotetrahedral symmetry, suggesting

(26) Frisch, M. J.; Trucks, G. W.; Schlegel, H. B.; Scuseria, G. E.; Robb, M. A.; Cheeseman, J. R.; Montgomery, J. A., Jr.; Vreven, T.; Kudin, K. N.; Burant, J. C.; Millam, J. M.; Iyengar, S. S.; Tomasi, J.; Barone, V.; Mennucci, B.; Cossi, M.; Scalmani, G.; Rega, N.; Petersson, G. A.; Nakatsuji, H.; Hada, M.; Ehara, M.; Toyota, K.; Fukuda, R.; Hasegawa, J.; Ishida, M.; Nakajima, T.; Honda, Y.; Kitao, O.; Nakai, H.; Klene, M.; Li, X.; Knox, J. E.; Hratchian, H. P.; Cross, J. B.; Bakken, V.; Adamo, C.; Jaramillo, J.; Gomperts, R.; Stratmann, R. E.; Yazyev, O.; Austin, A. J.; Cammi, R.; Pomelli, C.; Ochterski, J. W.; Ayala, P. Y.; Morokuma, K.; Voth, G. A.; Salvador, P.; Dannenberg, J. J.; Zakrzewski, V. G.; Dapprich, S.; Daniels, A. D.; Strain, M. C.; Farkas, O.; Malick, D. K.; Rabuck, A. D.; Raghavachari, K.; Foresman, J. B.; Ortiz, J. V.; Cui, Q.; Baboul, A. G.; Clifford, S.; Cioslowski, J.; Stefanov, B. B.; Liu, G.; Liashenko, A.; Piskorz, P.; Komaromi, I.; Martin, R. L.; Fox, D. J.; Keith, T.; Al-Laham, M. A.; Peng, C. Y.; Nanayakkara, A.; Challacombe, M.; Gill, P. M. W.; Johnson, B.; Chen, W.; Wong, M. W.; Gonzalez, C.; Pople, J. A. *Gaussian 03*, revision C.02; Gaussian, Inc.: Wallingford, CT, 2004.

(27) Parr; R. G. ; Yang; W. ; *Density-Functional Theory of Atoms and Molecules*; Oxford Univ. Press: Oxford; 1989.

(28) Stevens, W. J.; Krauss, M.; Basch, H.; Jasien, P. G. *Can. J. Chem.* **1992**, *70*, 612–630.

(29) Hirsekorn, K. F.; Veige, A. S.; Marshak, M. P.; Koldobskaya, Y.; Wolczanski, P. T.; Cundari, T. R.; Lobkovsky, E. B. *J. Am. Chem. Soc.* **2005**, *127*, 4809–4830.

(30) Vreven, T.; Morokuma, K. *J. Comput. Chem* **2000**, *21*, 1419–1432.

(31) Rappé, A. K.; Casewit, C. J.; Colwell, K. S.; Goddard, K. S., III.; Skiff, W. M. *J. Am. Chem. Soc.* **1992**, *114*, 10024–10035.

(32) Herzberg, G. *Molecular Spectra and Molecular Structure III. Electronic Spectra and Electronic Structure of Polyatomic Molecules, Reprint Edition*; Krieger: Malabar, 1991.

(33) Williams, D. S.; Schofield, M. H.; Anhaus, J. T.; Schrock, R. R. *J. Am. Chem. Soc.* **1990**, *112*, 6728–6729.

(34) Williams, D. S.; Schofield, M. H.; Schrock, R. R. *Organometallics* **1993**, *12*, 4560–4571.

(35) Williams, D. S.; Schrock, R. R. *Organometallics* **1993**, *12*, 1148–1160.

that strong π donors[36] may overcome the subtleties of $5d_{z^2}$/6s mixing. Whereas steric factors must also play a role in these systems, the lack of notable distortions in relatively low symmetry examples suggests that the pseudo-T_d environments are truly favored.

In homoleptic alkyl-[37] and aryl-thiolates,[38,39] subtle lowerings from T_d symmetry occur that render the complexes diamagnetic, which is also the case for D_{2d} $Mo(NMe_2)_4$.[40] For both types of complexes, PES spectra and calculations are consistent with a $^1A_1$ GS corresponding to the electronic configuration $(d_{x^2-y^2})^2$, and the energy gap to d_{z^2} is consistent with a splitting effected by π donation from the thiolate and amide ligands.[40,41] The related tungsten *tert*-butylthiolate complex, $W(S^tBu)_4$, possesses the same geometry and related electronic configuration as its molybdenum analogue.[42] In contrast, Schrock's virtually square-planar $W(O\text{-}2,6\text{-}C_6H_3{}^iPr_2)_4$ and $W(O\text{-}2,6\text{-}C_6H_3Me_2)_4$[42,43] serve as the predecessor to the aforementioned M(IV) tetraenolates.[42] A pseudo-tetrahedral geometry is available to the tetraphenoxide via an S_4 or related conformation, hence, this is another case where $5d_{z^2}$/6s mixing is important; however, the tetrathiolates do not suffer the same fate. Interelectronic repulsions are significantly greater for the larger sulfur atoms, providing an impetus toward tetrahedral geometry. In terms of energy, sulfur-based orbitals are more proximate to their metal counterparts than similar oxygen-derived ligands (i.e., ΔE_{ML} (sulfur-based) < ΔE_{ML} (oxygen-based)), a factor that contributes to bond-pair/bond pair repulsion. It is also difficult to assess the bonding differences between RS^- and RO^- without knowledge of overlap factors. Whereas one might tentatively assign the thiolate as the stronger field ligand, structural preferences based on the angular overlap model[24] do not favor either structure for a d^2 4-coordinate species when only σ bonding is considered. Because thiolates can essentially only π bond via one lone pair per sulfur, there is a modest π-bonding advantage to the tetrahedral structure, and the observed small distortions from T_d slightly enhance this difference. Unfortunately, direct comparisons to any 4-coordinate alkoxides or siloxides of interest have been hampered by aggregation.[44]

Conclusions

A comparison of experimental and computational metric parameters reveals that structural differences between Mo(IV) and W(IV) are primarily electronic in origin and that the relative energy of d_{z^2} is the major factor in determining (a) the propensity of molybdenum species toward tmp or pseudo-T_d conformations, and (b) the tendency of tungsten compounds toward squashed-T_d or distorted square-planar geometries. At the root of the structural differences is the greater $5d_{z^2}$/6s mixing for tungsten, which allows $5d_{z^2}$ to be low enough in energy to be occupied in the squashed-T_d geometry available to the 4-coordinate species. In the molybdenum cases, $4d_{z^2}$ is not pushed low enough in energy by mixing with the 5s orbital to permit the squashed-T_d geometry to be competitive with the pseudo-T_d, tmp triplet configurations. This work provides structural evidence for the influence of second-row versus third-row transition element $nd_{z^2}/(n+1)$s mixing and supports previous findings that the greater density of states (DOS) in second-row transition elements are partly responsible for their generally swifter reactivity than third-row elements.[10]

Experimental Section

General Considerations. All manipulations were performed using either glovebox or high vacuum line techniques. Hydrocarbon solvents containing 1−2 mL of added tetraglyme, and ethereal solvents were distilled under nitrogen from purple sodium benzophenone ketyl and were vacuum transferred from same prior to use. Benzene-d_6 was dried over activated 4 Å molecular sieves, vacuum transferred and stored under N_2. All glassware was oven-dried, and NMR tubes for sealed tube experiments were additionally flame-dried under dynamic vacuum. Gaseous reagents (ethylene, Matheson) were used as received and passed over a −78 °C trap prior to use. *trans*-$(Et_2O)_2MoCl_4$,[16] $MoCl_3(THF)_3$,[18] and *trans*-$Cl_4W(SEt_2)_2$[20] were prepared via literature routes.

NMR spectra were obtained using Varian XL-400, INOVA-400, and Unity-500 spectrometers, and chemical shifts are reported relative to benzene-d_6 (^1H, δ 7.15; $^{13}C\{^1H\}$, δ 128.39). Infrared spectra were recorded on a Nicolet Impact 410 spectrophotometer interfaced to a Gateway PC. Solution magnetic measurements were conducted via Evans' method.[17] Elemental analyses were performed by Oneida Research Services (Whitesboro, NY) or Robertson Microlit Laboratories (Madison, New Jersey).

Procedures. 1. (silox)$_3$MoCl$_2$ (1-Mo). To a 40 mL glass bomb reactor was added 2.00 g $^tBu_3SiONa$ (8.36 mmol) and 1.61 g $MoCl_4(OEt_2)$ (4.18 mmol). Twenty mL Et_2O was vacuum transferred into the bomb. The resulting suspension of red powder and green-brown solution was heated to 65 °C for 12 h. After cooling to 23 °C, the green reaction mixture was transferred from the bomb reactor, and all volatiles were removed. The filtrates were dissolved in pentane and filtered through a silica gel plug to give a yellow-brown solution. The solvent was removed in vacuo to give 0.340 g **1**-Mo as a yellow solid (15%). ^1H NMR (C_6D_6, 400 MHz): 2.46 ($\upsilon_{1/2} \approx 9$ Hz, 81H). $^{13}C\{^1H\}$ NMR (C_6D_6): 37.27 ($C(CH_3)$), 93.68 ($C(CH_3)$). Anal. Calcd $C_{36}H_{81}O_3Cl_2Si_3Mo$: C, 53.18; H, 10.04. Found: C, 53.11; H, 9.99.

2. (silox)$_3$MoCl (2-Mo). To a 100 mL glass bomb reactor containing 5.00 g $^tBu_3SiONa$ (20.9 mmol) and 2.69 g $MoCl_4(OEt_2)$ (6.97 mmol) was vacuum transferred 50 mL Et_2O at −78 °C. The resulting suspension of red powder in green-brown solution was heated to 100 °C for 12 h. After cooling the reaction mixture to 23 °C, the blue slurry was removed from the bomb reactor and filtered. The filter cake was washed 3 times with 25 mL Et_2O. Two equiv of PMe_3 were vacuum transferred to the blue filtrate via a gas bulb,

(36) (a) Cirera, J.; Ruiz, E.; Alvarez, S. *Inorg. Chem.* 2008, 47, in press.;(b) Cirera, J.; Alemany, P.; Alvarez, S. *Chem.—Eur. J.* **2004**, *10*, 190–207.
(37) Otsuka, S.; Kamata, M.; Hirotsu, K.; Higuchi, T. *J. Am. Chem. Soc.* **1981**, *103*, 3011–3014.
(38) Roland, E.; Walborsky, E. C.; Dewan, J. C.; Schrock, R. R. *J. Am. Chem. Soc.* **1985**, *107*, 5795–5797.
(39) Ueyama, N.; Zaima, H.; Nakamura, A. *Chem. Lett.* **1985**, 1481–1482.
(40) Chisholm, M. H.; Cotton, F. A.; Extine, M. W. *Inorg. Chem.* **1978**, *17*, 1329–1332.
(41) Takahashi, M.; Watanabe, I.; Ikeda, S.; Kamata, M.; Otsuka, S. *Bull. Chem. Soc. Jpn.* **1982**, *55*, 3757–3759.
(42) Listemann, M. L.; Dewan, J. C.; Schrock, R. R. *J. Am. Chem. Soc.* **1985**, *107*, 7207–7208.
(43) Listemann, M. L.; Schrock, R. R.; Dewan, J. C.; Kolodziej, R. M. *Inorg. Chem.* **1988**, *27*, 264–271.
(44) Chisholm, M. H.; Reichert, W. W.; Thornton, P. *J. Am. Chem. Soc.* **1978**, *100*, 2744–2748.

and aqua ((silox)$_3$ClMoPMe$_3$ (**2**-MoPMe$_3$)) precipitated from the green solution. The reaction mixture was cooled to −78 °C and filtered to give 3.52 g **2**-MoPMe$_3$ as an aqua solid. The solid was ground to a fine powder, loaded into a 100 mL round-bottom flask fitted with a 180° needle valve, and heated to 120 °C under dynamic vacuum for 4 h to give 3.25 g blue **2**-Mo (60% yield). ^{1}H NMR (C_6D_6): δ 3.27 ($\upsilon_{1/2} \approx 30$ Hz, 81H). ^{13}C{^{1}H} NMR (C_6D_6): δ 41.78 (*C*(CH$_3$)), 78.05 (C(*C*H$_3$)). Anal. Calcd for $C_{36}H_{81}ClMoO_3Si_3$: C, 55.60; H, 10.50. Found: C, 55.20; H, 10.30. μ_{eff} (293 K) = 2.4 μ_B (C_6D_6).

3. [(silox)$_2$MoCl]$_2$ (3-Mo). To a 150 mL glass bomb was added 3.08 g ^{t}Bu$_3$SiONa (12.9 mmol), 2.96 g MoCl$_3$(THF)$_3$ (7.10 mmol), and 50 mL THF via vacuum transfer at −78 °C. A red suspension darkened to brownish red upon warming. The reaction vessel was then placed in a 65 °C oil bath and allowed to stir for 12 h. It was removed from the oil bath, and the reaction mixture transferred to a 250 mL flask. The flask was evacuated, and the reaction mixture was stripped of all volatiles. The resulting brown solid was dissolved in 125 mL pentane and filtered away from the residual white precipitate. The filtrates were concentrated to ∼15 mL, cooled to −78 °C, and filtered to give 2.36 g (2.1 mmol, 65%) **3**-Mo as a brown microcrystalline solid. ^{1}H NMR (C_6D_6, 400 MHz): δ 1.25 (s, ^{t}Bu, 27H), 1.29 (s, ^{t}Bu, 27H). ^{13}C{^{1}H} NMR (C_6D_6): δ 23.98 (*C*(CH$_3$)), 24.53 (*C*(CH$_3$)), 30.98 (C(*C*H$_3$)), 31.67 (C(*C*H$_3$)). Anal. Calcd $C_{48}H_{108}Cl_2Mo_2O_4Si_4$: C, 51.27; H, 9.68. Found: C, 50.97; H, 9.53.

4. (silox)$_2$WCl$_4$ (4-W). To a 250 mL flask containing WCl$_6$ (10.00 g, 25.2 mmol) and ^{t}Bu$_3$SiOH (10.90 g, 50.4 mmol) was vacuum transferred 100 mL CCl$_4$ at −78 °C. Upon warming to 23 °C, the dark reddish-purple suspension formed a dark-red solution with the release of HCl gas. The reaction mixture was stirred at 23 °C for 3 h. The red solution with a small amount of dark precipitate was filtered, and the filtrates were concentrated to ∼15 mL. The filtrates were cooled to 0 °C and filtered to give deep-red microcrystals of (^{t}Bu$_3$SiO)$_2$WCl$_4$ (17.30 g, 90%). ^{1}H NMR (C_6D_6): δ 1.38 (s, ^{t}Bu). ^{13}C{^{1}H} NMR (C_6D_6): δ 27.23 (*C*(CH$_3$)), 32.55 (C(*C*H$_3$)). Anal. Calcd $C_{24}H_{54}O_2Si_2Cl_4W$: C, 38.10; H, 7.19. Found: C, 37.89; H, 6.85.

5. (silox)$_3$WCl$_2$ (1-W). a. To a bomb reactor charged with WCl$_4$(SEt$_2$)$_2$ (3.90 g, 7.71 mmol) and 2.00 equiv of Tl(silox) (6.45 g, 15.42 mmol) was added 100 mL benzene. The reactor was heated to 100 °C for 3 days, and a tan solid and burgundy solution were observed. The volatiles were removed and the solids were triturated with hexanes (3 × 20 mL) and placed under vacuum for 12 h. A mixture of hexanes and benzene were used to remove the reaction mixture, and it was filtered through celite. After removal of the volatiles, hexanes were used to chromatograph the mixture using silica (in air). The dichloride was isolated from hexanes as a microcrystalline pink solid (2.81 g, 41%).

b. Via (silox)$_2$WCl$_3$ (5-W). To a 500 mL round-bottom flask containing 10.00 g (13.2 mmol) **4**-W and 34.89 g (14.4 mmol) 0.95% Na/Hg was distilled 200 mL Et$_2$O. The red suspension slowly turned to a green-blue solution after stirring at 23 °C for 30 min. The reaction mixture was filtered, and the filtrates were concentrated to 20 mL. Cooling to −78 °C followed by filtration gave 9.05 g (95%) **5**-W as a green-blue solid (tentative formulation based on the following data. ^{1}H NMR (C_6D_6, 400 MHz): 1.61 ($\upsilon_{1/2}$∼40 Hz, 81H). Anal. Calcd $C_{24}H_{54}Cl_3O_2Si_2W$: C, 39.98; H, 7.55. Found: C 39.27; H, 9.96.). To a 200 mL glass bomb charged with 8.00 g **5**-W (11.1 mmol) and 3.98 g ^{t}Bu$_3$SiONa (16.6 mmol) was vacuum transferred 100 mL Et$_2$O at −78 °C. The reaction mixture was warmed to 23 °C and allowed to stir in a 70 °C oil bath for 4 h. The red reaction mixture was transferred to a 250 mL flask and stripped of all volatiles. The pink residue was dissolved in 200 mL hexanes and filtered through a plug of silica gel to give a pink-red solution. The hexanes were removed in vacuo to give 9.50 g **1**-W (95%). ^{1}H NMR (C_6D_6): δ 2.29 ($\upsilon_{1/2} \approx 20$ Hz, 81H, C(*CH*$_3$)).^{13}C{^{1}H} NMR (C_6D_6): δ 36.39 (*C*(*C*H$_3$)), 70.78 (*C*(CH$_3$)). UV−vis (CH_2Cl_2, nm): 238 (ϵ = 9700 M^{-1}cm^{-1}), 265 (ϵ = 7700 M^{-1}cm^{-1}), 296 (ϵ = 6500 M^{-1}cm^{-1}), 528 (ϵ = 190 M^{-1}cm^{-1}), 625 (ϵ = 20 M^{-1}cm^{-1}). Anal. Calcd for $C_{36}H_{81}O_3Si_3Cl_2W$: C, 48.0; H, 9.0. Found: C, 47.4; H, 8.7.

6. (silox)$_3$WCl (2-W). To a 50 mL flask charged with **1**-W (800 mg, 0.89 mmol) and 1.5 equiv Na/Hg (0.80% Na, 31 mg, 1.33 mmol Na, 3.83 g Hg) was added 20 mL THF by distillation at −78 °C. The reaction mixture was allowed to warm to 23 °C, and turned blue during the course of stirring for 30 min. The volatiles were removed, and the solids were triturated with hexanes (3 × 5 mL) followed by removal of the volatiles. The excess mercury was decanted, and the crude material dissolved in hexanes and crystallized at −78 °C to afford green microcrystals (500 mg, 65%). ^{1}H NMR (C_6D_6): δ 1.34 (s, 81H, C(*CH*$_3$)). ^{13}C{^{1}H} NMR (C_6D_6): δ 28.38 (*C*(CH$_3$)) 34.50 (C(*C*H$_3$)). UV−vis (hexanes, nm): 236 (ϵ = 2600 M^{-1}cm^{-1}), 266 (ϵ = 2350 M^{-1}cm^{-1}), 312 (ϵ = 1600 M^{-1}cm^{-1}), 376 (ϵ = 640 M^{-1}cm^{-1}), 635 (ϵ = 70 M^{-1}cm^{-1}). Anal. Calcd for $C_{36}H_{81}O_3Si_3ClW$: C, 52.1; H, 9.8. Found: C, 48.31, 49.92; H, 9.11, 8.96.

7. (silox)$_3$MoMe (2-MoMe). To a 25 mL flask equipped with a stir bar was added 0.200 g **2**-Mo (0.257 mmol) and 10 mL Et$_2$O via vacuum transfer at −78 °C. The slurry was allowed to warm, the resulting blue solution was cooled to −78 °C, and 0.095 mL CH$_3$MgBr (3.0 M in Et$_2$O) was added via syringe. The reaction mixture was allowed to warm to 23 °C over the course of 2 h and was stirred for an additional 2 h. The maroon reaction mixture was filtered, and the filtrate was reduced in volume to ∼1 mL. Dark-red microcrystals were crystallized from the filtrate at −78 °C and collected by cold filtration (0.136 g, 70%). ^{1}H NMR (C_6D_6, 400 MHz): δ 2.88 ($\upsilon_{1/2} \approx 76$ Hz, C(*CH*$_3$)). ^{13}C{^{1}H} NMR (C_6D_6): δ 47.66 (CH$_3$, $\upsilon_{1/2}$ = 9 Hz), 280 (CH$_3$, $\upsilon_{1/2}$ = 118 Hz). Anal. Calcd: $C_{37}H_{84}O_3Si_3Mo$: C, 58.68; H, 11.18. Found: C, 58.29; H, 10.98. μ_{eff} (293 K) = 2.5 μ_B (C_6D_6).

8. (silox)$_3$MoH (2-MoH). To a 25 mL flask equipped with a stir bar was added 0.500 g **2**-Mo (0.643 mmol) and ∼10 mL Et$_2$O via vacuum transfer at −78 °C. The blue solution was cooled to −78 °C, and 1.0 mL Na[Et$_3$BH] (1.0 M in toluene) was added via syringe. The reaction mixture was allowed to warm to 23 °C over the course of 2 h and was stirred for an additional 3 h. The brown reaction mixture was filtered, and the filtrates reduced in volume to ∼2 mL. The filtrates were cooled to −78 °C, and the resulting reddish-brown microcrystals were collected by cold filtration to yield 0.253 g of **2**-MoH (53%). ^{1}H NMR (C_6D_6, 400 MHz): δ 2.91 ($\upsilon_{1/2} \approx 53$ Hz, C(*CH*$_3$)). ^{13}C{^{1}H} NMR (C_6D_6): δ 31.44 (*C*(CH$_3$)), 54.64 (C(*C*H$_3$)). IR (nujol mull, Na/Cl) 1884 υ(MoH) = 1884 cm^{-1}. Anal. Calcd: $C_{36}H_{82}O_3Si_3Mo$: C, 58.18; H, 11.12 Found: C, 57.83; H, 10.76. μ_{eff} (293 K) = 2.6 μ_B (C_6D_6).

9. (silox)$_3$MoCH$_2$CH$_3$ (2-MoEt). a. To a 25 mL round-bottom flask containing 0.200 g **2**-Mo (0.257 mmol) was distilled ∼10 mL Et$_2$O. The blue solution was cooled to −78 °C, and 0.095 mL CH$_3$CH$_2$MgBr (3 M in Et$_2$O) was added via syringe. The reaction mixture was stirred as it warmed to 23 °C over the course of 2 h and was stirred for an additional 2 h. The maroon reaction mixture was filtered and the filtrates reduced in volume to ∼1 mL. Yellow-green microcrystals were crystallized from the filtrates at −78 °C and collected by cold filtration (0.143 g, 72%).

b. To a 40 mL glass bomb reactor equipped with a stir bar was added a solution of 0.250 g **2**-MoH (0.336 mmol) in ∼10 mL

benzene. The solution was degassed, and 10 equiv of ethylene transferred via a calibrated gas bulb. The bomb containing the brown solution was then heated to 100 °C in an oil bath for 12 h, and the solution slowly changed to dark yellow. The reaction mixture was stripped of all volatiles, giving a dark yellow-green solid. The product was dissolved in minimal Et_2O, and the resulting solution was allowed to evaporate slowly at −30 °C. After ∼12 h, yellow-green crystals were collected by decanting the mother liquor (0.221 g, 85%). ^{1}H NMR (C_6D_6): δ 2.77 ($\upsilon_{1/2} \approx$ 68 Hz, 81H, C(CH_3)). ^{13}C{^{1}H} NMR (C_6D_6): δ 48.39 (C(CH_3)$_3$, $\upsilon_{1/2}$ = 15 Hz), 276 (SiC, $\upsilon_{1/2}$ = 115 Hz). Anal. Calcd for $C_{38}H_{86}MoO_3Si_3$: C, 59.17; H, 11.24. Found: C, 58.89; H, 10.97. μ_{eff} (293 K) = 2.5 μ_B (C_6D_6).

10. (silox)$_3$WCH$_3$ (2-WMe). To a 50 mL flask charged with 0.500 g **2**-W (0.577 mmol) was added 20 mL Et_2O by vacuum transfer at −78 °C. The blue solution was cooled to −78 °C, and 0.211 mL CH_3MgBr (3.0 M in Et_2O, 1.1 equiv) was added via syringe. The reaction mixture was allowed to warm to 23 °C over the course of 3 h, and was stirred at 23 °C for an additional 10 min. The maroon reaction mixture was filtered, and the volatiles were removed. The dark purple solid was dissolved in minimal Et_2O and the resulting solution allowed to slowly evaporate to give purple microcrystals (0.195 g, 40%). ^{1}H NMR (C_6D_6): δ 3.69 ($\upsilon_{1/2}$ = 7 Hz, C(CH_3)). Anal. Calcd for $C_{37}H_{84}O_3Si_3Mo$: C, 49.95; H, 10.02. Found: C, 49.51; H, 9.65. μ_{eff} (293K) = 1.5 μ_B (C_6D_6).

11. (silox)$_3$WCH (6-W). To a 50 mL glass bomb containing 0.500 g **2**-WMe (0.592 mmol) was vacuum transferred 10 mL C_6H_6. The reaction vessel was placed in a 75 °C oil bath and allowed to stir for 24 h. It was removed from the oil bath, and the reaction mixture was transferred to a 50 mL round-bottom flask. The reaction mixture was stripped of all volatiles and washed with 5 mL cold pentane to give 0.474 g **6**-W (95%). ^{1}H NMR (C_6D_6, 400 MHz): δ 1.27 (s, ^{t}Bu, 81H), 6.03 (s, $^2J_{WH}$ = 69 Hz, CH, 1H). ^{13}C{^{1}H} NMR (C_6D_6): δ 24.48 (*C*(CH$_3$)), 31.10 (C(*C*H$_3$)), 271.64 (WC). Anal. Calcd $C_{37}H_{82}O_3Si_3W$: C, 52.71; H, 9.80. Found: C, 52.48; H, 9.54.

Magnetic Susceptibility Measurements. Magnetic susceptibility measurements of crystalline powdered samples (20−30 mg) were performed on a Quantum Design MPMS-5 SQUID magnetometer at 10 kOe between 5 and 300 K for all samples. All sample preparations and manipulations were performed under an inert atmosphere because of the air sensitivity of the samples. The samples were either measured in a flame-sealed NMR tube or a custom machined-sealed Teflon capsule. The diamagnetic contribution from the sample container was subtracted from the experimental data. Pascal's constants[33] were used to subtract diamagnetic contributions, yielding paramagnetic susceptibilities.

Single-Crystal X-Ray Diffraction Studies. Upon isolation, the crystals were covered in polyisobutylene and placed under a 173 °C N_2 stream on the goniometer head of a Siemens P4 SMART CCD area detector system (graphite-monochromated Mo Kα, λ= 0.71073 Å). The structures were solved by direct methods (*SHELXS*). All non-hydrogen atoms were refined anisotropically unless stated, and hydrogen atoms were treated as idealized contributions.

12. (silox)$_3$MoCl (2-Mo). A blue block (0.3 × 0.10 × 0.05 mm) was obtained from benzene. A total of 31 393 reflections were collected with 11 023 determined to be symmetry independent (R_{int} = 0.0509), and 7685 were greater than 2σ(*I*). The data was corrected for absorption by *SADABS*, and the refinement utilized $w^{-1} = \sigma^2(F_o^2) + (0.0322p)^2 + 8.4454p$, where $p = (F_o^2 + 2F_c^2)/3$).

13. (silox)$_3$WCl$_2$ (1-W). A pink crystal was obtained from THF. A total of 5247 reflections were collected with 5216 being symmetry independent (*I*), with R_{int} = 0.0208) and 3668 were greater than 2σ(*I*). The data was corrected for absorption by *SADABS*, and the refinement utilized $w^{-1} = \sigma^2(F_o^2) + (0.0756p)^2 + 0.0000p$, where $p = (F_o^2 + 2F_c^2)/3$). The low level of data prompted isotropic refinement of peripheral carbon (^{t}Bu) atoms; core atoms were refined anisotropically. A disordered THF molecule was *SQUEEZd*.

14. (silox)$_3$WCl (2-W). A blue-green block (0.3 × 0.2 × 0.15) was obtained from hexanes. A total of 10 249 reflections were collected with 6859 being symmetry independent (*I*), with R_{int} = 0.0294) and 5259 were greater than 2σ(*I*). The data was corrected for absorption by *SADABS*, and the refinement utilized $w^{-1} = \sigma^2(F_o^2) + (0.0180p)^2 + 6.1390p$, where $p = (F_o^2 + 2F_c^2)/3$).

15. (silox)$_3$MoEt (2-MoEt). A dark-green block (0.3 × 0.2 × 0.1) was obtained from benzene. A total of 48 709 reflections were collected with 9043 being symmetry independent (*I*), with R_{int} = 0.0341) and 8064 were greater than 2σ(*I*). The data was corrected for absorption by *SADABS*, and the refinement utilized $w^{-1} = \sigma^2(F_o^2) + (0.0849p)^2 + 9.0484p$, where $p = (F_o^2 + 2F_c^2)/3$). A disordered benzene solvent molecule resides at the center of symmetry of the cell.

16. (silox)$_3$WMe (1-WMe). A black block (0.3 × 0.2 × 0.1) was obtained from diethyl ether. A total of 30 004 reflections were collected with 6400 being symmetry independent (*I*), with R_{int} = 0.0682) and 4909 were greater than 2σ(*I*). The data was corrected for absorption by *SADABS*, and the refinement utilized $w^{-1} = \sigma^2(F_o^2) + (0.0481p)^2 + 22.0459p$, where $p = (F_o^2 + 2F_c^2)/3$). Refinement was somewhat hampered by a whole molecule disorder (major/minor = 95:5).

Computational Methods. Calculations were performed on full silox-decorated models using the *Gaussian03* package.[26] Density functional theory (DFT), specifically the BLYP functional, was utilized for all simulations.[27] The transition metals and heavy main group atoms (silicon and phosphorus) were described with the Stevens effective core potentials (ECPs) and attendant valence basis sets (VBSs).[28] This scheme, dubbed CEP-31G, entails a valence triple-ζ description for the transition metals, and a double-ζ VBS for the main group elements. The 6−31G(d) all-electron basis set was used for carbon, hydrogen, and oxygen atoms. All main group VBSs are augmented with a d polarization function (C(ξ_d) = 0.8; Si(ξ_d) = 0.3247; P(ξ_d) = 0.37). This level of theory was selected on the basis of a series of test calculations on the singlet and triplet states of Nb(OH)$_3$, Ta(OH)$_3$,[11] and their olefin adducts.[29]

Full silox models were studied using hybrid quantum mechanics/molecular mechanics (QM/MM) techniques within the *ONIOM* framework.[30] The QM region of M(silox)$_3$(X) complexes contained the transition metal, the oxygen and silicon atoms of the silox group, and the entire X group (if present). The QM level of theory employed is that described above. The remainder of the molecule, that is, the *tert*-butyl groups of silox was modeled with the universal force field (UFF).[31]

Full geometry optimizations without any metric or symmetry restrictions were employed to obtain the minima in this research. All of the resultant stationary points were characterized as true minima (i.e., no imaginary frequencies) by calculation of the energy Hessian. Enthalpic and entropic corrections to the total electronic energy were calculated using harmonic vibrational frequencies determined at the same level of theory employed for geometry optimization and are calculated at 1 atm and 298.15 K.

Closed- and open-shell species were described with the restricted and unrestricted Kohn−Sham formalisms, respectively, with no evidence of spin contamination for the latter.

Acknowledgment. We thank the National Science Foundation (CHE-0415506, (P.T.W.)), the U.S. Dept. of Energy (DE-FG02-03ER15387 (TRC)), and Cornell University for financial support; R.E.D. thanks the Lindemann Trust for a Fellowship.

Supporting Information Available: CIF files of **1**-Mo (CCDC 660935), **1**-W (CCDC 660934), **2**-W, **2**-MoEt (CCDC 660937), **2**-WMe (CCDC 660939). This material is available free of charge via the Internet at http://pubs.acs.org.

IC800139C